UNLIMITED
UNCLASSIFIED

Canada

(6)

SKIN FRICTION MEASUREMENTS FOR TWO RELATIVELY THICK AIRFOIL SECTIONS AT HIGH REYNOLDS NUMBER

by

G. M. Elfstrom

National Aeronautical Establishment

AERONAUTICAL NOTE
NAE-AN-23
NRC NO. 23941

OTTAWA
NOVEMBER 1984

National Research Council Canada
Conseil national de recherches Canada

NATIONAL AERONAUTICAL ESTABLISHMENT

SCIENTIFIC AND TECHNICAL PUBLICATIONS

AERONAUTICAL REPORTS:

Aeronautical Reports (LR): Scientific and technical information pertaining to aeronautics considered important, complete, and a lasting contribution to existing knowledge.

Mechanical Engineering Reports (MS): Scientific and technical information pertaining to investigations outside aeronautics considered important, complete, and a lasting contribution to existing knowledge.

AERONAUTICAL NOTES (AN): Information less broad in scope but nevertheless of importance as a contribution to existing knowledge.

LABORATORY TECHNICAL REPORTS (LTR): Information receiving limited distribution because of preliminary data, security classification, proprietary, or other reasons.

Details on the availability of these publications may be obtained from:

Publications Section,
National Research Council Canada,
National Aeronautical Establishment,
Bldg. M-16, Room 204,
Montreal Road,
Ottawa, Ontario
K1A 0R6

ÉTABLISSEMENT AÉRONAUTIQUE NATIONAL

PUBLICATIONS SCIENTIFIQUES ET TECHNIQUES

RAPPORTS D'AÉRONAUTIQUE

Rapports d'aéronautique (LR): Informations scientifiques et techniques touchant l'aéronautique jugées importantes, complètes et durables en termes de contribution aux connaissances actuelles.

Rapports de génie mécanique (MS): Informations scientifiques et techniques sur la recherche externe à l'aéronautique jugées importantes, complètes et durables en termes de contribution aux connaissances actuelles.

CAHIERS D'AÉRONAUTIQUE (AN): Informations de moindre portée mais importantes en termes d'accroissement des connaissances.

RAPPORTS TECHNIQUES DE LABORATOIRE (LTR): Informations peu disséminées pour des raisons d'usage secret, de droit de propriété ou autres ou parce qu'elles constituent des données préliminaires.

Les publications ci-dessus peuvent être obtenues à l'adresse suivante:

Section des publications
Conseil national de recherches Canada
Établissement aéronautique national
Im. M-16, pièce 204
Chemin de Montréal
Ottawa (Ontario)
K1A 0R6

UNLIMITED
UNCLASSIFIED

SKIN FRICTION MEASUREMENTS FOR TWO RELATIVELY THICK AIRFOIL SECTIONS AT HIGH REYNOLDS NUMBER

MESURES DU FROTTEMENT SUR DEUX PROFILS AÉRODYNAMIQUES ASSEZ ÉPAIS À NOMBRES DE REYNOLDS ÉLEVÉS

by/par

G.M. Elfstrom

National Aeronautical Establishment

AERONAUTICAL NOTE
NAE-AN-23
NRC NO. 23941

OTTAWA
NOVEMBER 1984

L.H. Ohman, Head/Chef
High Speed Aerodynamic Laboratory/
Laboratoire d'aérodynamique à hautes vitesses

G.M. Lindberg
Director/Directeur

ABSTRACT

An experimental investigation of turbulent skin friction for two airfoil sections under conditions of high Reynolds number is described. Data are presented for an NACA 0020 section at a Mach number of 0.30 and chord Reynolds numbers between 5 and 20 million, and for a 16% thick supercritical section at a Mach number of 0.74 and chord Reynolds numbers between 15 and 25 million. Together with estimates of boundary layer transition location, these data are integrated to determine the skin friction component of total drag. The results are then discussed in terms of observed variation of total drag with Reynolds number.

RÉSUMÉ

Il s'agit d'une recherche expérimentale ayant trait au frottement turbulent sur deux profils aérodynamiques à nombres de Reynolds élevés. Les données sont présentées pour un profil NACA 0020 à un nombre de Mach de 0.30 et à des nombres de Reynolds au niveau de la corde compris entre 5 et 20 millions, et pour un profil supercritique d'une épaisseur de 16% à un nombre de Mach de 0.74 et à des nombres de Reynolds au niveau de la corde compris entre 15 et 25 millions. Ces données, combinées avec estimations de l'emplacement de transition de la couche limite, sont intégrées pour déterminer la composante de frottement de la traînée totale. Les résultats sont ensuite étudiés en fonction de la variation de la traînée totale observée en fonction du nombre de Reynolds.

CONTENTS

TABLES

ILLUSTRATIONS

ILLUSTRATIONS (Cont'd)

SYMBOLS

Symbol	Definition
B	model span
c	model chord
C_D'	integrand for wake drag coefficient
C_{DF}	skin friction drag coefficient = $[\int C_f d(x/c)]\cos\alpha$
C_{DP}	pressure drag coefficient = $[\int C_p d(y/c)]\cos\alpha$
C_{DWi}	wake drag coefficient as determined from traverse of probe "i" = $\int_i C_D' d(h/c)$
C_{DW}	arithmetic mean of three C_{DWi}
C_f	skin friction coefficient = τ/q
C_{LP}	lift coefficient from integrated surface pressure = $[\int C_p d(x/c)]\cos\alpha - [\int C_p d(y/c)]\sin\alpha$
C_p	surface pressure coefficient = $(p - p_\infty)/q_\infty$
d	trip wire diameter
h	obstacle-block diameter; also vertical position of wake rake from tunnel centreline
M	Mach number
m	non-dimensional pressure gradient parameter in Falkner-Skan representation of boundary layer ($U_e \sim s^m$)
p	pressure

SYMBOLS (Cont'd)

Symbol	Definition
q	dynamic pressure = $\frac{1}{2}\rho U^2$ (Q in Fig. 5)
R	radius of curvature
Re_c	chord Reynolds number = $U_\infty c/\upsilon_\infty$
Re_s	Reynolds number based on arc length from stagnation point = $U_e s/\upsilon_e$
Re_{δ_o}	Reynolds number based on local boundary layer thickness = $U_e \delta_o/\upsilon_e$
s	arc length from stagnation point
t	model thickness
u'	root-mean-square of U_∞ fluctuation
U	velocity in streamwise direction
x,y	airfoil surface co-ordinates relative to chordline
X^x, Y^x	obstacle-block calibration parameters
α	angle of incidence (corrected) = ALPHAC in Table 2
δ	boundary layer thickness
ρ	density
υ	kinematic viscosity
τ_w	shear stress at model surface
	Subscripts, Superscripts and Prefixes
b	conditions associated with obstacle block
B	derived from sidewall balance measurements
e	shear layer edge conditions
F	derived from integrated skin friction
i	incompressible conditions
LE	leading edge
o	stagnation or reference conditions
P	derived from integrated static pressure

SYMBOLS (Cont'd)

Symbol	Definition
	Subscripts, Superscripts and Prefixes
prof	profile, i.e. total, drag
s	conditions ahead of normal shock-wave
TE	trailing edge
w	wall-temperature conditions; also conditions at height 'd' in boundary layer
'	fluctuating quantities (root-mean-square)
*	sonic conditions
∞	freestream static conditions
Δ	increment in, or correction to, a quantity

SKIN FRICTION MEASUREMENTS FOR TWO RELATIVELY THICK AEROFOIL SECTIONS AT HIGH REYNOLDS NUMBER

1.0 INTRODUCTION

A large proportion of airfoil drag is due to viscous surface shear, particularly under cruise conditions. Measurement of local skin friction coefficient distribution can therefore be very helpful in the interpretation of measured drag of new airfoil sections. In addition, it will help in the experimental verification of specific design features. To be of most use, such data should be obtained under the high Reynolds number conditions characteristic of flight. The NAE 15-in. X 60-in. test facility (Ref. 1) has such a capability. This report discusses skin friction measurements taken on two airfoil models, covering a wide Reynolds number range.

The airfoil sections studied are both relatively thick — a classical one (NACA 0020) intended for low speed conditions, and another (16% thick supercritical) designed for high speed. Details of the latter are presented in Reference 2, however two features are worth discussing since they relate to skin friction. First, there is a favourable pressure gradient over a significant portion of the nose, and second, there is a concave-shaped trailing edge. The intent of the first feature was to delay the onset of boundary layer transition as far as possible, thus minimizing skin friction drag. The second feature was a consequence of the first — to compensate for the loss of lift due to reduced leading-edge suction, the upper surface suction region had to be extended rearwards. To reduce the likelihood of boundary layer separation due to the short recovery region, a concave pressure distribution was employed for both the upper and lower rear surfaces.

This report will discuss the skin friction measurements taken using models of these airfoil sections in the NAE 15-in. X 60-in. test facility. These data will serve as a base for checking several boundary layer prediction methods and airfoil flowfield prediction methods which have boundary layer codes imbedded in them. Finally, the skin friction distributions will be integrated to yield skin friction drag, thereby providing some insight into sources of total drag.

2.0 EXPERIMENTAL PROCEDURE

In this section key details concerning models, determination of drag, determination and control of transition and method of measuring local skin friction will be given.

2.1 Airfoil Models

Both models spanned the 15-in. width of the test section. They had 'hydraulically smooth' surfaces (surface finish of 10-15 μ · in.) — with an equivalent sand-grain roughness Reynolds number of about 30 at most, this is well below the critical level (p. 515, Ref. 3) for roughness effects to be significant.

The supercritical airfoil model, like most tested in the facility, has a chord of 10 inches. Static orifices of 0.0145-in. diameter were installed in two rows straddling the centreline, 80 in all. For the purpose of finding the location of boundary layer transition a 'trip strip' made up by glueing grit on the model surface was occasionally employed.

The NACA 0020 model had a much larger chord (15 inches) in order to achieve chord Reynolds number, Re_c, of 10×10^6 without resorting to short run times at low Mach number. Static orifices 0.020-in. diameter straddled the centreline in two rows. For some tests a 'trip wire' 0.010-in. diameter was glued to both surfaces at $x/c = 0.05$.

2.2 Determination of Airfoil Drag

For both models the standard sidewall-mounted traversing rake was used to measure drag by wake momentum traverse. In this experiment, as is common in most conducted in the facility, the arithmetic mean value of drag obtained from three probes was used to represent sectional drag. Typical drag polars obtained using these data are presented in Figures 1 and 2. The rather large data scatter exhibited for the NACA 0020 model was due to pneumatic response problems present in the rake system at the time these tests were conducted — subsequent improvements have considerably reduced such scatter.

Within the expected uncertainty, there was no significant variation in drag coefficient as indicated by individual rake probes in the NACA 0020 model tests. This was not always the case in that of the supercritical airfoil model tests. At high M_∞, particularly at the higher lift coefficient, there was a monotonic decrease from C_{DW1} to C_{DW3}, e.g. 0.0010 at $M_\infty \simeq 0.74$, $Re_c = 20 \times 10^6$, $C_L \simeq 0.3$. This decrement was found to correlate with strength of a shock-wave, when present. This observation is mentioned here in the context of interpreting skin friction drag, as obtained from skin friction measured near the model centreline. The evidence suggests that the three-dimensional nature of the shock interacting with the sidewall boundary layer produces the observed C_{DWi} non-uniformity, and not, say, due to the non-uniform transition location due to the tripping effect of the static orifices located on centreline. We will return to this later, in Section 5.0.

2.3 Determination and Fixing of Transition

The scope of skin friction measurement was limited to the turbulent flow regime, and so some check on the existence of turbulent flow was deemed necessary, particularly in the case of the supercritical airfoil model which was designed with a long region of laminar flow. Two detection methods were employed — observation of total drag variations with a 'trip-strip' affixed at different locations, and surface oil flow visualization.

Details of the applied strip are given in Figure 3 — for consistency, a strip was applied to both upper and lower surfaces at a given location. A trip strip rather than a trip wire was chosen because this was easier to remove and re-apply between tunnel runs. The principle of diagnosis was as follows: with the trip well forward, the total drag would be quite high due partly to the trip drag and partly to the increased length of turbulent flow; as the trip is moved aft, the drag would decrease due to a shorter length of turbulent flow; once within the naturally turbulent region there would be little or no further change in drag for quite some distance. As seen in Figure 3, the trend is the reverse of that indicated above. Undoubtedly an over-riding effect is the change in trip drag with location — the local dynamic pressure *increases* continually (favourable pressure gradient). Unfortunately, the drag coefficient of the trip is not known, so it is not possible to extract location of natural transition from these data. (If the airfoil had a long region of essentially zero pressure gradient, it would have been possible to do so.) In future experiments it may be feasible to effectively utilize this technique on a given airfoil, provided a special investigation is carried out which will yield the trip drag coefficient under various local Mach number and Reynolds number conditions.

Some limited results were obtained using surface oil flow visualization. A certain degree of caution is required here since the oil flow itself can influence the transition process. With this in mind a very thin layer off oil/kerosene mixture tinted with a small amount of lamp-black was used. This was painted on the model between 2% and 10% chord just prior to a tunnel run, then the model was preset to a given incidence and exposed to a 10-second run. Afterwards the flow pattern was observed — unfortunately, the resultant patterns were too difficult (faint) to photograph. The transition region was taken to be the chordal area where the turbulent wedges tended to coalesce. Observed locations of transition, on both upper and lower model surfaces, are shown in Figure 4 for three test conditions. For comparison purposes, predictions of the start of transition are also indicated in the figure. The theory is that due to Van Driest and Blumer (Ref. 4) which includes the influence of longitudinal surface pressure gradient and freestream turbulence — details of its application are provided in Appendix I. The actual turbulence level, measured by the author, was typically 0.3% to

0.5%. Figure 4 provides two interesting observations in this context: the prediction method is adequate if a mean value of 0.4% is assumed for the freestream turbulence level, and if the turbulence level were near zero, transition would probably be almost twice as far aft of that observed. We will return to the latter observation later. Other test conditions were also checked in this manner — results not shown — and the same agreement between theory and experiment was observed.

Equivalent predictions were made for the NACA 0012 case — oil flow visualization was not carried out, in the interest of expediency. The predicted start of transition for zero model incidence is shown in Figure 5 for 0.4% and 1% turbulence. Also shown in the figure is information concerning the trip wire employed in these tests. The relations for estimating trip wire drag — needed in the interpretation of total drag — follow those due to Koslov (Ref. 5). For the purpose of estimating transition location when the trip wire was on, we can use the analysis procedure given by Schlichting (Ref. 3, p. 512). The wire Reynolds number was at lowest about 4000 — thus transition is predicted to be complete within six wire diameters at most, and so the transition location was taken to be the wire location at all test conditions.

2.4 Measurement of Turbulent Skin Friction

Skin friction data were determined from measurements taken using a device called the congruent obstacle back. This is one of a family of devices which stagnate the flow at the model surface and through use of so-called wall similarity parameters indicate skin friction indirectly. For a detailed discussion of this device, Reference 6 should be consulted.

The obstacle block was chosen over the more classical Preston tube because of its ease of consistent application and it inherently accounts for the influence of static hole error. A sketch showing geometry of the device and a summary of the calibration relations are given in Figure 6. For computation of "wall" conditions, the adiabatic wall temperature was used, assuming a recovery factor of 0.89. Note Y_i^* is the equivalent incompressible value of Y^* for a given X^*. A point of qualification here is that the value of X^* typical in these experiments is about 8, which is outside the range used in the calibration (Ref. 6).

Measurements were obtained using both airfoil models at three Reynolds numbers, with fixed Mach number. The mechanics of obtaining skin friction data were as follows:

- "clean" model surface static pressure data were obtained for those test conditions where skin friction data were desired.
- obstacle blocks were then affixed to the model surface congruent with selected static pressure orifices. Placement of a given block in relation to others followed the guidelines presented in Reference 6.
- the model was tested again, several times at each test condition, during which the obstacle blocks would be moved to various locations.
- after the required testing was complete (typically four tunnel runs for a given M_∞ and Re_c), the pressure rise, Δp, due to the presence of each obstacle block was found by subtracting the clean wing pressure value from that with the block affixed.
- for the NACA 0020 model, a saving in testing was made possible due to the symmetrical airfoil shape. The model was pitched symmetrically through zero incidence so that both "upper" and "lower" surface pressure distributions could be obtained in one tunnel run. In this way the number of runs required was cut in half.

Skin friction data were not corrected for longitudinal static pressure gradient effects since no technique is available for the obstacle block. However, some indication of the magnitude of likely corrections can be obtained by calculating those for a Preston tube of equivalent size. According to the correlation derived by Frei (Ref. 7) the maximum likely correction in the present tests would be 0.7%, which is negligible.

3.0 DISCUSSION OF SKIN FRICTION RESULTS

In this section the static pressure and skin friction measurements will be presented. Some comparison with theoretical predictions will be made, including those which predicts the entire flowfield, not just skin friction. The data obtained for the supercritical airfoil model are also used to verify certain design features.

3.1 NACA 0020 Airfoil Model

Tests were carried out at $M_\infty = 0.30$ under Re_c conditions of 5×10^6, 10×10^6 and 20×10^6. Three values of incidence were chosen: 0°, 4.5° and 8.9°. The static pressure distributions obtained are presented in Figure 7, for the case without trip wire present. Equivalent data with the trip wire on are virtually indistinguishable, except adjacent to the wire itself. The influence of Reynolds number is very weak, limited to the trailing edge region at 0° and 4.5° incidence. At the highest incidence, Figure 7(c), there is a "plateau" in the pressure distribution near the trailing edge on the upper surface, indicative of a small separation region.

In Figure 7(a) through (c) are shown several predictions, whose sophistication increases with increasing incidence. At zero incidence, the potential flow prediction agrees very well with the measured data, except near the trailing edge. This is, of course, expected at high Reynolds number. At 4.5° incidence — Figure 7(b) — the vortex-panel method of Choo (Ref. 8) agrees well with measured data on the upper surface, but not as well on the lower surface. This situation is accentuated at the highest incidence — Figure 7(c). The method has the option of including a separated flow bubble, however this resulted in only a slight improvement, as seen in the figure. Also shown are predictions due to Reference 9. The agreement is clearly superior. Note: the legend shows the names of the authors attributed to the prediction methods, including the authors attributed to the boundary layer calculation methods imbedded therein (Refs. 10 and 11).

Skin friction measurements taken *without* the trip wire affixed are presented in Figures 8(a) through (c). Full tabulated data are listed in Tables 2-1 through 2-12. Two key features of the data are that, as expected, the skin friction coefficient is reduced at high Reynolds number, and that at the highest incidence there is a region of essentially zero skin friction near the trailing edge, confirming the diagnosis of a separated flow.

Also shown in Figures 8(a) through (c) are predictions which use the *measured* Cp data as input. Both methods (Refs. 12 and 13) need a location of transition specified. For this the method of Van Driest and Blumer (Ref. 4) was used, with a freestream turbulence value of 0.4% assumed, as discussed previously. In Figure 8(c) both Green's and Cebeci's methods fail to predict the observed flow separation region at the highest incidence. This is a problem common to most prediction methods — the reduced pressure gradient near separation is taken to be a relaxation, and so C_f is not further reduced.

Corresponding C_f data obtained with the trip wire *on* are presented in Figures 9(a) through (c), along with trip off data for comparison. Only data for $Re_c = 5 \times 10^6$ were obtained with the trip wire on, due to time constraints. The first observation to be made is that due to the forced location of transition, C_f is in general lower with the trip wire on. In order to substantiate the negative C_f values indicated at the highest incidence, a few runs were carried out with some obstable blocks yawed 180°, i.e. facing rearwards. For this orientation, a positive Δp was taken, by definition, to indicate negative C_f. The results, shown in Figure 9(c) indicate just that. Thus, while the absolute value of C_f is undoubtedly in question due to a vanishing small "logarithmic" region of the velocity profile, the results demonstrate that the obstacle block can serve to indicate the presence of flow separation.

Results of C_f predictions using Cebeci's method are shown in Figures 9(a) through (c). In all cases where the trip wire was used, transition was assumed to start at the trip itself. In general, the predictions agree quite well with measurement, the exception being the separated flow region at the highest incidence. Also shown in Figure 9(b) are the predicted results using Choo's method (Ref. 8). In this case the "input" pressure distribution is the predicted one, shown earlier (Fig. 7(b)).

Coincidentally, the strong adverse pressure gradient on the upper surface near the trailing edge produces a near-zero C_f there, as found in the experiment. Analogous results for the highest model incidence are shown in Figure 9(d); the corresponding predicted pressure distributions were shown in Figure 7(c). The results show that inclusion of the separated flow option does not significantly improve Choo's predictions.

3.2 Supercritical Airfoil Model

Four values of model incidence were tested, with natural transition only. Pressure and skin friction data are tabulated in Tables 2-13 through 2-24. Both Cp and C_f distributions are plotted in Figure 10(a) through (d), without any theoretical predictions included.

Regarding key features, the first observation to make is that the Cp data show the shock wave, when it is present, moves rearward very slightly as Reynolds number is increased. This is confirmed by the C_f data, e.g. Figure 10(b) upper plot. The second observation is that C_f is in general reduced as Reynolds number increases. Figures 10(c) and (d) illustrate very markedly in the C_f distributions the strong "recovery" region downstream of the shock wave. This recovery is present even at the maximum lift condition — Figure 10(d). Finally, the concave trailing edge pressure distribution shows a slightly improved "recovery" as Re_c increases, and under none of the conditions tested does there appear to be any flow separation in that region of the airfoil. Since the skin friction is quite low there, a few runs were made with the obstacle blocks yawed 180°. It was found that the Δp was always negative for any block location over the last 10% of chord, thus confirming the non-existence of reversed (separated) flow.

A few comparisons with results from a flow-field prediction code were made — Choo's and Cebeci's methods are for incompressible flow and thus are not valid here. The one chosen (Ref. 14) was in fact used in the process of checking the design of this airfoil, and so is pertinent. Imbedded in this method is Nash's boundary layer calculation scheme. Skin friction predictions using this combination are compared with the present data in Figure 11. The agreement is obviously poor. In an effort to improve the prediction, the more advanced boundary layer calculation method of Green (Ref. 13) was substituted for Nash's method and the calculation re-run. While the results, shown in Figure 11, indicate significant improvement, the agreement is still not very good. To be fair, it should be noted that this test condition was very close to maximum lift, and thus it must impose a very stringent test of the flow-field prediction code. It is important to note that C_L, not α was the specified input parameter. As evident in Figure 12, the trailing-edge Cp recovery is over-predicted, so under the total lift matching constraint the suction region Cp was under-predicted. Since the boundary layer property predictions are of more direct interest in this report, a check on Green's method was made under less stringent conditions — lower lift coefficient using the measured pressure distribution. This is illustrated in Figure 13. Clearly the agreement is much better.

Recently, a number of flow-field prediction methods which deal only with the shock-boundary layer interaction itself have appeared. The present C_f data provide a useful test case for one particular ultimate predictive capability — incipient separation. The data show that this condition ($C_f \rightarrow 0$) occurs at an incidence equal to (or perhaps just greater than) the third highest of the four tested. To a first approximation, this is not a function of Re_c. This then defines the maximum Mach number, M_s, just ahead of the shock wave which will not cause the boundary layer to separate. This value (1.275) is shown in Figure 14 along with two predictions (Refs. 15 and 16). Of the two, the method of Behning and Zierep better predicts this incipient separation condition.

4.0 SKIN FRICTION DRAG

Since turbulent skin friction accounts for the major portion of the skin friction drag of these airfoils, it is a logical next step to in fact compute the skin friction drag. This quantity, C_{DF}, is found simply by performing a contour integration around the airfoil (see the list of symbols). The procedure used was as follows:

- in the laminar and transition regions the C_f values there were those predicted by Cebeci, (Ref. 12).
- the location of transition was defined in the manner discussed in Section 2.3.
- skin friction in the turbulent region was that as measured.
- the contour integral was performed using a simple numerical scheme, after which the resultant drag coefficient was multiplied by the cosine of model incidence.

Results for the NACA 0020 airfoil model are shown in Figure 15: part (a) is natural flow, part (b) is with the trip wire installed. The first observation to be made is that C_{DF} is only a weak function of lift, unlike total drag which is a strong function of lift. The second point of note concerns the data where the trip wire was not installed — results for the intermediate Reynolds number are consistently greater than those at the higher and lower Reynolds numbers. The location of transition plays a key role here, and it appears that its movement with Re_c determines C_{DF} variations to a large extent. Although complimentary data are not available for the case where the trip wire was attached, it can be safely presumed that C_{DF} would decrease monotomically as Re_c is increased, due to the fixed location of transition.

Skin friction drag results for the supercritical airfoil are shown in Figure 16. Here again the variation with lift is very slight. The trend with Re_c is not clear, due to the data scatter. This in turn could be due to a high sensitivity of transition location to slight variations in pressure gradient.

5.0 INTERPRETATION OF TOTAL DRAG

In this section we will show how knowledge of skin friction drag helps to understand observed trends in total drag with Re_c. A few comments will then be made on the extrapolation of these results to free air (flight) conditions.

Knowledge of the transition location is important, because the absolute level of skin friction drag is directly related to the transition location. In this regard, the question arises as to the relevance of comparing skin friction drag, C_{DF}, with the three-probe average value of total drag, C_{DW}. In the case of the NACA 0020 model results, there should be no difficulty, since all three probes yield essentially the same value of drag coefficient. However, in the case of the supercritical airfoil model, for the test conditions presented here, there is a distinct non-uniformity — mentioned earlier, in Section 2.2. So as not to confuse possible mean shock-strength variations with those "seen" on centreline (where the static orifices are), it is recommended that only C_{DW1} data be used for this airfoil. Logically, it also makes sense from another viewpoint — if the static orifices do cause premature transition to turbulent flow, as suggested in Reference 17, then C_{DW1} results in part from skin friction drag in the vicinity of the (centreline) static orifices. A plot showing C_{DW1} variations with C_{LP} and Re_c is given in Figure 17.

5.1 NACA 0020 Airfoil Model

In the case where the trip wire is affixed, the interpretation of total drag variations with Re_c is relatively straight-forward. Even in the absence of skin friction data at Re_c other than 5×10^6, it can safely be assumed that the majority of the reduction in C_{DW} with increasing Re_c is the direct result of the reduction in turbulent skin friction. Some reduction might also be due to improvement in trailing-edge pressure recovery, but the effect is small, as mentioned in Section 3.1. Likewise for the variation of the trip wire drag itself — according to the formula given in Figure 5, the trip drag, $\Delta C_{D_{WIRE}}$, is reduced only 0.0002 between Re_c of 5×10^6 and 20×10^6.

For the "clean" airfoil, the total drag was seen to be almost the same at $Re_c = 5 \times 10^6$ and 20×10^6, but higher at 10×10^6 — see Figure 1. The same trend was evident in the skin friction drag — see Figure 15. Thus again it appears that skin friction drag controls total drag; in this case the movement in transition location essentially counteracts the direct effect of local turbulent skin friction coefficient changes.

What then of the difference between total drag, trip wire on vs off? This is best discussed in terms of components, as shown graphically in Figure 18. First of all, the drag due to two trip wires is about 12 "counts" (0.0012) according to Reference 5. After subtracting that plus the measured skin friction drag, the residual amount will represent the implied pressure drag C_{DP}. Note that C_{DP} is significantly larger with the trip wire on. The included plot of trailing edge pressure distribution suggests that lower pressure recovery explains the larger C_{DP} with the trip wire on. This seems reasonable because the trailing edge boundary layer should be much thicker in that case.

Extrapolation to flight conditions in general implies variation with Reynolds number and freestream conditions. If the test Reynolds number range is sufficiently high, such that transition occurs well forward on the airfoil, then the extrapolation on the basis of Re_c is straightforward. This is true for both clean-airfoil data and trip-on data. However, even in the present experiments, where Re_c is very high, the extrapolation to flight conditions on the basis of freestream turbulence level is not entirely clear. As an aid in this, consider drag predictions using the ESDV data sheets (Ref. 18). For these predictions the location of transition was taken to be that given by Reference 4, as shown in Figure 5. Results are shown in Figure 19. It is interesting to note that, first of all, the overall level of agreement with measurements is quite good. Note also that both theory and experiment show a reversal in trend with Re_c for the clean wing, this being a result of the shift in transition location. Assuming that the prediction of transition location in free air (zero turbulence level) is correct, it is obvious that there is quite a difference in drag to be expected between the wind tunnel and free air cases. This difference should diminish at the higher Reynolds number.

5.2 Supercritical Airfoil Model

Unlike the NACA 0020 model results, the supercritical airfoil model drag data decreased continuously with Re_c. While this might be expected on the basis of a reduction in turbulent skin friction, the measured C_{DF} showed no significant change at all. As explained in the previous discussion, it is apparent that the forward shift in transition location is counteracting the reduction in C_f. This leaves only C_{DP} variations to be responsible for the observed reduction.

There is a clear improvement in the trailing edge pressure recovery with increasing Re_c, as seen in Figure 20. Although a discussion of the details are beyond the scope of this report, estimates of C_{DP} were made, incorporating a correction for laminar and turbulent static orifice pressure error. The resulting values, which agreed with $C_{DW_1} - C_{DF}$ to within ±0.0005, confirmed this trend in C_{DW_1}. It is to be noted that in comparison with the NACA 0020 model, C_{DP} is almost twice as large, while C_{DF} is only slightly larger. Thus it is to be expected that changes in C_{DF} will dominate trends with Re_c.

There remains the question of freestream turbulence in terms of extrapolation to flight conditions. This will, of course, affect the skin friction drag predominantly. A rough estimate for the change in C_{DF} can be obtained by calculating the reduction in C_{DF} due to a more aft location of transition — see Figure 4 — using the measured C_f distributions. At $Re_c = 10 \times 10^6$, C_{DF} and thus C_{DW} would be reduced about 0.0010.

6.0 RECOMMENDATIONS

From the convenience of testing viewpoint, it is recommended that static orifices be installed in several rows, well separated laterally, so as to permit simultaneous use of many obstacle blocks. In this way the number of runs required to obtain a complete C_f distribution could be minimized. A side benefit of this in general would be a reduction in the risk of premature transition due to the tripping effect of the holes. A further improvement in this latter regard would be to utilize smaller orifice sizes. However, if skin friction measurement using obstacle blocks are to be taken seriously, this is not recommended, as the orifice size used (0.0145 in.) in the present experiments is realistically a minimum due to the handling/mounting problems associated with the small blocks.

The remainder of the recommendations concern the subject of transition, particularly in the context of calculating skin friction drag. Firstly, a simple reliable method of detecting transition location is desirable. This will allow the user to affix blocks only where needed, i.e. in the turbulent flow region only. A trip can serve as a detection tool because transition occurs very close to it at the high Reynolds numbers typical of normal test conditions. However, it is very important to know what the drag coefficient of the trip itself is. This may, in the case of compressible flow, necessitate a special experiment conducted on, say, a flat plate under similar conditions, e.g. trip height in relation to boundary layer thickness, local Mach number etc. Oil flow visualization is somewhat difficult at high Reynolds number due to its affect on the very thin boundary layers typically present.

An alternative to detecting transition is prediction, particularly in the context of extrapolation to flight (zero turbulence) conditions. It is interesting to note that in recent literature, e.g. Reference 19, there is evidence that transition location may be very much further aft in flight than previously thought — transition has occurred at $Re_x = 6 \times 10^6$, much higher than that predicted by Reference 4 and other contemporary methods.

7.0 CONCLUSIONS

The obstacle block technique has been used to measure turbulent skin friction on two relatively thick airfoil section models in the NAE 15-in. X 60-in. 2-0 test section. The test conditions ranged from essentially incompressible to highly compressible, at high Reynolds number. The resulting skin friction data were useful in the following ways:

- confirmation of the presence of flow separation at the trailing edge of the NACA 0020 at high incidence
- confirmed a design feature of the supercritical airfoil, that of a separation-free trailing edge
- provided data suitable for the determination of skin friction drag. Due to occasionally sparse data and uncertainty in the local of transition, the absolute value of C_{DF} is in some doubt. However the results proved useful in explaining trends with Reynolds number.

8.0 ACKNOWLEDGEMENTS

The author would like to thank the David W. Taylor Naval Ship Research and Development Center and the De Havilland Aircraft of Canada Ltd. for loan of the NACA 0020 and 16% supercritical airfoil models, respectively. The skill and patience of Mr. G. Lanouette (now retired) of the NAE in the development of techniques for affixing exceedingly small obstacle blocks is greatly appreciated. Further thanks go to Mr. D.J. Jones of the NAE and Mr. D. Choo for providing flowfield calculations on the NACA 0020 airfoil, and to Mr. R. Poole of De Havilland for the same on the supercritical airfoil.

9.0 REFERENCES

1. Ohman, L.H. — *The Role of the NAE 5-foot X 5-foot Wind Tunnel in the Development of Modern Airfoil Sections.* CASI J., Vol. 22, No. 1, 1976, pp. 1-22.

2. Eggleston, B. Jones, D.J. Elfstrom, G.M. — *Development of Modern Airfoil Sections for High Subsonic Cruise Speeds.* AIAA Paper 79-0687, 1979.

3. Schlichting, H. — *Boundary Layer Theory.* McGraw-Hill, N.Y., 6th ed. 1968.

4. Van Driest, E.R. Blumer, C.B. — *Boundary Layer Transition: Freestream Turbulence and Pressure Gradient Effects.* AIAA J., Vol. 1, 1963, pp. 1303-1306.

5. Koslov, L.F. — *Investigation of the Boundary Layer Turbulence Stimulation of the Ship Models.* Proc. 12th ITTC, Rome, 1969.

6. Elfstrom, G.M. Kostopoulos, C. Peake, D.J. Fisher, D. — *The Obstacle Block as a Device to Measure Turbulent Skin Friction in Compressible Flow.* AIAA Paper 82-0589, 1982.

7. Frei, D. Thomann, H. — *Direct Measurements of Skin Friction in a Turbulent Boundary Layer with a Strong Adverse Pressure Gradient.* J. Fluid Mech., Vol. 101, pt. 1, 1980, pp. 79-95.

8. Choo, D.O. — *Predicting Multi-Element Airfoil Flows — Final Report.* NRC Contract #1Sx78-0083, HiTech Canada Ltd., Feb. 1980.

9. Bauer, F. Garabedian, F. Jameson, A. Korn, D. — *Supercritical Wing Sections II, a Handbook.* Lecture Notes in Economic and Mathematical Systems, Vol. 108, Springer-Verlag, 1975.

10. Head, M.R. — *Entrainment in the Turbulent Boundary Layer.* ARC R&M 3152, 1958.

11. Nash, J.F. Macdonald, A.G.J. — *The Calculation of Momentum Thickness in a Turbulent Boundary Layer at Mach Numbers up to Unity.* ARC Cp No. 963, 1967.

12. Cebeci, T. Bradshaw, P. — *Momentum Transfer in Boundary Layers.* McGraw-Hill, 1977.

13. Green, J.E. Weeks, D.J. Brooman, F.W.F. — *Prediction of Turbulent Boundary Layers and Wakes in Compressible Flow by a Lag-Entrainment Method.* RAE-TR 72231, 1973.

14. Bauer, F. Garabedian, F. Korn, D. — *Supercritical Wing Sections III.* Lecture Notes in Econ. and Math, Syst., Vol. 150, Springer-Verlag, 1977.

15. Liou, M.S. Adamson, T.C. — *Interaction Between a Normal Shock Wave and a Turbulent Boundary Layer at High Transonic Speeds. Part II: Wall Shear Stress.* J. Appl. Math. & Phys. (ZAMP), Vol. 31, 1980, pp. 227-246.

16. Bohning, R. Zierep, J. — *Normal Shock-Boundary Layer Interaction at a Curved Wall.* Paper 17, AGARD-CP-291, 1980.

17. Somers, D.M. Stack, J.P. Harvey, W.D. — *Influence of Surface Static-Pressure Orifices on Boundary Layer Transition.* NASA-TM-84492, July 1982.

18. Anon — *Profile Drag of Smooth Aerofoils with Straight Trailing Edges at Low Speeds.* Data Sheets Wings 02.04.03 and 02.04.01, Amended, ESDU Ltd., 1978.

19. Winter, K.G. Maskell, E.C. — *The Reynolds Number for Transition on a Flat Plate in the RAE 4-ft X 3-ft Low Turbulence Wind Tunnel.* RAE TM Aero 1854, 1980.

TABLE 1

CENTRELINE HOT FILM TURBULENCE MEASUREMENTS IN EMPTY TUNNEL

M_∞	$Re_c^* \times 10^{-6}$	u'/U_∞ (%)
0.74	16.0	0.34
0.74	14.5	0.29
0.74	12.8	0.27
0.77	14.5	0.47
0.75	14.5	0.47
0.73	14.5	0.50
0.71	14.5	0.48
	(mean)	0.41

* equivalent to the 10-inch chord model tested

u'/U_∞ represents r.m.s. quantities (bandwidth 30 Hz — 15 kHz) derived from mass flux fluctuations according to the method of W.C. Rose & E.P. McDaid, AIAA J., Vol. 15, pp. 1368-1370, 1977.

TABLE 2-01

NACA 0020 AIRFOIL MODEL

M	REC	ALPHAC	CL(B)	CL(P)
0.298	5.2E06	0.06	-0.002	0.005

Upper Surface			Lower Surface		
X/C	CP	CF	X/C	CP	CF
0.980	0.208	0.00092	0.000	1.019	
0.970	0.175	0.00116	0.010	0.154	
0.960	0.161		0.020	-0.104	
0.950	0.118		0.040	-0.381	
0.940	0.110		0.050	-0.508	
0.930	0.096		0.060	-0.588	
0.920	0.089		0.070	-0.631	
0.910	0.067		0.080	-0.671	
0.900	0.043		0.090	-0.699	
0.880	0.004	0.00200	0.100	-0.700	
0.860	-0.024		0.125	-0.725	
0.830	-0.064		0.150	-0.725	
0.800	-0.081	0.00221	0.175	-0.720	
0.750	-0.120	0.00260	0.200	-0.706	
0.700	-0.166	0.00269	0.225	-0.677	
0.600	-0.268		0.250	-0.645	
0.500	-0.374	0.00307	0.275	-0.618	
0.450	-0.429		0.300	-0.591	
0.400	-0.492	0.00517	0.350	-0.553	0.00453
0.350	-0.536	0.00438	0.400	-0.500	0.00524
0.300	-0.622		0.450	-0.446	
0.275	-0.639		0.500	-0.389	0.00321
0.250	-0.660		0.600	-0.272	
0.225	-0.690		0.700	-0.166	0.00269
0.200	-0.708		0.750	-0.111	0.00251
0.175	-0.729		0.800	-0.052	0.00192
0.150	-0.744		0.830	-0.025	
0.125	-0.741		0.860	0.005	
0.100	-0.715		0.880	0.014	0.00190
0.090	-0.710		0.900	0.048	
0.080	-0.680		0.910	0.064	
0.070	-0.654		0.920	0.086	
0.060	-0.612		0.930	0.120	
0.050	-0.540		0.940	0.135	
0.040	-0.438		0.950	0.158	
0.030	-0.290		0.960	0.179	
0.020	-0.087		0.970	0.195	0.00094
0.010	0.165		0.980	0.244	0.00052

TABLE 2-02

NACA 0020 AIRFOIL MODEL

M	REC	ALPHAC	CL(B)	CL(P)
0.298	5.2E06	4.56	0.394	0.404

Upper Surface			Lower Surface		
X/C	CP	CF	X/C	CP	CF
0.980	0.227	0.00072	0.010	0.733	
0.970	0.208	0.00039	0.020	0.592	
0.960	0.205		0.040	0.275	
0.950	0.189		0.050	0.144	
0.940	0.163		0.060	0.048	
0.930	0.151		0.070	-0.011	
0.920	0.138		0.080	-0.072	
0.910	0.107		0.090	-0.123	
0.900	0.090		0.100	-0.166	
0.880	0.053	0.00124	0.125	-0.264	
0.860	0.018		0.150	-0.307	
0.830	-0.029		0.175	-0.342	
0.800	-0.082	0.00173	0.200	-0.352	
0.750	-0.165	0.00219	0.225	-0.351	
0.700	-0.229	0.00215	0.250	-0.357	
0.600	-0.374		0.275	-0.354	
0.500	-0.526	0.00298	0.300	-0.352	
0.450	-0.594		0.350	-0.352	
0.400	-0.687	0.00436	0.400	-0.322	0.00585
0.350	-0.775	0.00443	0.450	-0.290	
0.300	-0.869		0.500	-0.267	0.00450
0.275	-0.921	0.00601	0.600	-0.200	
0.250	-0.964		0.700	-0.147	0.00339
0.225	-1.019		0.750	-0.107	0.00301
0.200	-1.063	0.00639	0.800	-0.066	0.00292
0.175	-1.173		0.830	-0.047	
0.150	-1.234		0.860	-0.007	
0.125	-1.297		0.880	0.018	0.00237
0.100	-1.344		0.900	0.039	
0.090	-1.366		0.910	0.045	
0.080	-1.357		0.920	0.055	
0.070	-1.361		0.930	0.067	
0.060	-1.390		0.940	0.081	
0.050	-1.362		0.950	0.099	
0.040	-1.340		0.960	0.112	
0.030	-1.250		0.970	0.145	0.00184
0.020	-1.101		0.980	0.180	0.00096
0.010	-0.936				
0.000	0.800				

TABLE 2-03

NACA 0020 AIRFOIL MODEL

M	REC	ALPHAC	CL(B)	CL(P)
0.298	5.2E06	8.86	0.805	0.820

Upper Surface			Lower Surface		
X/C	CP	CF	X/C	CP	CF
0.980	0.236	-.00069	0.020	0.941	
0.970	0.208	0.00013	0.040	0.745	
0.960	0.204		0.050	0.641	
0.950	0.186		0.060	0.555	
0.940	0.184		0.070	0.487	
0.930	0.154		0.080	0.413	
0.920	0.130		0.090	0.356	
0.910	0.124		0.100	0.306	
0.900	0.096		0.125	0.180	
0.880	0.074	0.00003	0.150	0.102	
0.860	0.024		0.175	0.033	
0.830	-0.035		0.200	-0.014	
0.800	-0.064	0.00112	0.225	-0.036	
0.750	-0.151	0.00142	0.250	-0.059	
0.700	-0.231	0.00172	0.275	-0.071	
0.600	-0.398		0.300	-0.084	
0.500	-0.617	0.00264	0.350	-0.103	
0.450	-0.725		0.400	-0.110	
0.400	-0.843	0.00381	0.450	-0.122	
0.350	-0.976	0.00401	0.500	-0.108	
0.300	-1.124		0.600	-0.074	
0.275	-1.185	0.00485	0.700	-0.041	0.00359
0.250	-1.296		0.750	-0.018	0.00373
0.225	-1.389		0.800	-0.005	0.00324
0.200	-1.475	0.00637	0 330	-0.008	
0.175	-1.606		0.860	0.005	
0.150	-1.711	0.00964	0.880	-0.007	0.00357
0.125	-1.818		0.900	0.008	
0.100	-1.959		0.910	0.023	
0.090	-2.061		0.920	0.021	
0.080	-2.156		0.930	0.031	
0.070	-2.237		0.940	0.016	
0.060	-2.330		0.950	0.043	
0.050	-2.427		0.960	0.069	
0.040	-2.442		0.970	0.079	0.00223
0.030	-2.485		0.980	0.121	0.00198
0.020	-2.517				
0.010	-2.539				
0.000	0.081				
0.010	0.998				

TABLE 2-04

NACA 0020 AIRFOIL MODEL

M	REC	ALPHAC	CL(B)	CL(P)
0.299	10.0E06	0.05	0.005	0.005

Upper Surface			Lower Surface		
X/C	CP	CF	X/C	CP	CF
0.980	0.225	0.00070	0.000	1.029	
0.970	0.198	0.00093	0.010	0.163	
0.960	0.164		0.020	-0.097	
0.950	0.131		0.040	-0.386	
0.940	0.109		0.050	-0.528	
0.930	0.086		0.060	-0.591	
0.920	0.079		0.070	-0.613	
0.910	0.055		0.080	-0.641	
0.900	0.053		0.090	-0.665	
0.880	0.016	0.00179	0.100	-0.700	
0.860	-0.014		0.125	-0.731	
0.830	-0.049		0.150	-0.735	
0.800	-0.090	0.00211	0.175	-0.730	
0.750	-0.148	0.00220	0.200	-0.706	0.00458
0.700	-0.200	0.00240	0.225	-0.694	
0.600	-0.301		0.250	-0.671	
0.500	-0.404	0.00306	0.275	-0.646	0.00613
0.450	-0.456		0.300	-0.623	
0.400	-0.514	0.00446	0.350	-0.581	0.00391
0.350	-0.564	0.00378	0.400	-0.519	0.00450
0.300	-0.605		0.450	-0.464	
0.275	-0.647	0.00614	0.500	-0.409	0.00310
0.250	-0.697		0.600	-0.297	
0.225	-0.716		0.700	-0.194	0.00234
0.200	-0.734	0.00478	0.750	-0.144	0.00216
0.175	-0.747		0.800	-0.086	0.00208
0.150	-0.746		0.830	-0.050	
0.125	-0.749		0.860	-0.005	
0.100	-0.721		0.880	0.033	0.00165
0.090	-0.712		0.900	0.066	
0.080	-0.679		0.910	0.077	
0.070	-0.640		0.920	0.099	
0.060	-0.607		0.930	0.108	
0.050	-0.531		0.940	0.128	
0.040	-0.437		0.950	0.151	
0.030	-0.276		0.960	0.179	
0.020	-0.102		0.970	0.211	0.00081
0.010	0.171		0.980	0.248	0.00047

TABLE 2-05

NACA 0020 AIRFOIL MODEL

M	REC	ALPHAC	CL(B)	CL(P)
0.299	10.0E06	4.51	0.419	0.426

Upper Surface			Lower Surface		
X/C	CP	CF	X/C	CP	CF
0.980	0.251	0.00026	0.010	0.793	
0.970	0.227	0.00039	0.020	0.584	
0.960	0.199		0.040	0.278	
0.950	0.174		0.050	0.142	
0.940	0.152		0.060	0.063	
0.930	0.135		0.070	-0.005	
0.920	0.107		0.080	-0.069	
0.910	0.089		0.090	-0.114	
0.900	0.074		0.100	-0.114	
0.880	0.030	0.00144	0.125	-0.230	
0.860	-0.003		0.150	-0.289	
0.830	-0.054		0.175	-0.318	
0.800	-0.097	0.00177	0.200	-0.336	
0.750	-0.175	0.00195	0.225	-0.355	
0.700	-0.250	0.00227	0.250	-0.360	
0.600	-0.396		0.275	-0.363	0.00661
0.500	-0.547	0.00314	0.300	-0.353	
0.450	-0.626		0.350	-0.351	0.00369
0.400	-0.704	0.00374	0.400	-0.333	0.00630
0.350	-0.808	0.00389	0.450	-0.295	
0.300	-0.909		0.500	-0.267	0.00301
0.275	-0.947	0.00438	0.600	-0.211	
0.250	-0.997		0.700	-0.147	0.00293
0.225	-1.070		0.750	-0.108	0.00243
0.200	-1.116	0.00544	0.800	-0.065	0.00245
0.175	-1.166		0.830	-0.034	
0.150	-1.223	0.00624	0.860	0.000	
0.125	-1.284		0.880	0.021	0.00203
0.100	-1.345		0.900	0.045	
0.090	-1.357		0.910	0.049	
0.080	-1.360		0.920	0.064	
0.070	-1.374		0.930	0.078	
0.060	-1.385		0.940	0.082	
0.050	-1.377		0.950	0.112	
0.040	-1.341		0.960	0.132	
0.030	-1.256		0.970	0.165	0.00122
0.020	-1.142		0.980	0.201	0.00094
0.010	-0.994				
0.000	0.786				

TABLE 2-06

NACA 0020 AIRFOIL MODEL

M	REC	ALPHAC	CL(B)	CL(P)
0.299	10.0E06	8.78	0.847	0.843

Upper Surface			Lower Surface		
X/C	CP	CF	X/C	CP	CF
0.980	0.208	0.00010	0.020	0.949	
0.970	0.201	0.00009	0.040	0.741	
0.960	0.190		0.050	0.625	
0.950	0.178		0.060	0.542	
0.940	0.164		0.070	0.479	
0.930	0.154		0.080	0.413	
0.920	0.137		0.090	0.346	
0.910	0.124		0.100	0.295	
0.900	0.116		0.125	0.181	
0.880	0.070	0.00065	0.150	0.106	
0.860	0.031		0.175	0.056	
0.830	-0.028		0.200	-0.001	
0.800	-0.088	0.00119	0.225	-0.026	
0.750	-0.173	0.00134	0.250	-0.059	
0.700	-0.269	0.00173	0.275	-0.071	
0.600	-0.450		0.300	-0.084	
0.500	-0.647	0.00276	0.350	-0.107	
0.450	-0.757		0.400	-0.109	0.00571
0.400	-0.870	0.00323	0.450	-0.108	
0.350	-1.000	0.00363	0.500	-0.113	0.00388
0.300	-1.146		0.600	-0.089	
0.275	-1.225	0.00388	0.700	-0.061	0.00350
0.250	-1.330		0.750	-0.044	0.00252
0.225	-1.431		0.800	-0.021	0.00296
0.200	-1.527	0.00583	0.830	-0.005	
0.175	-1.627		0.860	0.006	
0.150	-1.749	0.00677	0.880	0.024	0.00238
0.125	-1.885		0.900	0.039	
0.100	-2.034		0.910	0.043	
0.090	-2.114		0.920	0.052	
0.080	-2.160		0.930	0.047	
0.070	-2.224		0.940	0.036	
0.060	-2.331		0.950	0.054	
0.050	-2.400		0.960	0.057	
0.040	-2.473		0.970	0.077	0.00203
0.030	-2.482		0.980	0.107	0.00183
0.020	-2.485				
0.010	-2.631				
0.000	0.076				
0.010	1.007				

TABLE 2-07

NACA 0020 AIRFOIL MODEL

M	REC	ALPHAC	CL(B)	CL(P)
0.297	19.8E06	0.06	-0.001	-0.004

Upper Surface			Lower Surface		
X/C	CP	CF	X/C	CP	CF
0.980	0.245	0.00067	0.000	1.027	
0.970	0.208	0.00074	0.010	0.156	
0.960	0.171		0.020	-0.125	
0.950	0.134		0.040	-0.384	
0.940	0.119		0.050	-0.509	
0.930	0.103		0.060	-0.578	
0.920	0.085		0.070	-0.628	
0.910	0.060		0.080	-0.651	
0.900	0.057		0.090	-0.690	
0.880	0.027	0.00154	0.100	-0.700	
0.860	-0.005		0.125	-0.729	
0.830	-0.047		0.150	-0.746	0.00482
0.800	-0.081	0.00184	0.175	-0.735	
0.750	-0.140		0.200	-0.719	0.00425
0.700	-0.193	0.00212	0.225	-0.700	
0.600	-0.294		0.250	-0.673	
0.500	-0.399	0.00278	0.275	-0.653	0.00361
0.450	-0.454		0.300	-0.622	
0.400	-0.515	0.00329	0.350	-0.580	0.00343
0.350	-0.577	0.00341	0.400	-0.523	0.00333
0.300	-0.625		0.450	-0.469	
0.275	-0.648	0.00358	0.500	-0.409	0.00285
0.250	-0.675		0.600	-0.295	
0.225	-0.701		0.700	-0.189	0.00209
0.200	-0.714	0.00420	0.750	-0.139	
0.175	-0.728		0.800	-0.085	0.00187
0.150	-0.731	0.00469	0.830	-0.047	
0.125	-0.729		0.860	-0.001	
0.100	-0.693		0.880	0.027	0.00154
0.090	-0.675		0.900	0.064	
0.080	-0.649		0.910	0.077	
0.070	-0.616		0.920	0.096	
0.060	-0.575		0.930	0.109	
0.050	-0.518		0.940	0.118	
0.040	-0.424		0.950	0.157	
0.030	-0.273		0.960	0.181	
0.020	-0.085		0.970	0.203	0.00078
0.010	0.168		0.980	0.248	0.00064

TABLE 2-08

NACA 0020 AIRFOIL MODEL

M	REC	ALPHAC	CL(B)	CL(P)
0.297	19.8E06	4.50	0.433	0.426

Upper Surface			Lower Surface		
X/C	CP	CF	X/C	CP	CF
0.980	0.268	0.00022	0.010	0.799	
0.970	0.247	0.00037	0.020	0.601	
0.960	0.222		0.040	0.280	
0.950	0.190		0.050	0.143	
0.940	0.173		0.060	0.056	
0.930	0.144		0.070	-0.015	
0.920	0.131		0.080	-0.068	
0.910	0.102		0.090	-0.100	
0.900	0.080		0.100	-0.074	
0.880	0.044	0.00117	0.125	-0.225	
0.860	0.006		0.150	-0.283	0.00456
0.830	-0.042		0.175	-0.313	
0.800	-0.077	0.00148	0.200	-0.343	0.00368
0.750	-0.166		0.225	-0.347	
0.700	-0.233	0.00191	0.250	-0.350	
0.600	-0.367		0.275	-0.356	0.00385
0.500	-0.531	0.00263	0.300	-0.352	
0.450	-0.608		0.350	-0.339	0.00320
0.400	-0.702	0.00321	0.400	-0.318	0.00314
0.350	-0.795	0.00344	0.450	-0.288	
0.300	-0.897		0.500	-0.255	0.00268
0.275	-0.942	0.00374	0.600	-0.189	
0.250	-1.009		0.700	-0.127	0.00219
0.225	-1.066		0.750	-0.083	
0.200	-1.117	0.00477	0.800	-0.049	0.00204
0.175	-1.178		0.830	-0.026	
0.150	-1.239	0.00536	0.860	0.017	
0.125	-1.289		0.880	0.031	0.00182
0.100	-1.338		0.900	0.053	
0.090	-1.360		0.910	0.061	
0.080	-1.377		0.920	0.073	
0.070	-1.375		0.930	0.087	
0.060	-1.391		0.940	0.092	
0.050	-1.372		0.950	0.117	
0.040	-1.328		0.960	0.146	
0.030	-1.222		0.970	0.173	0.00114
0.020	-1.015		0.980	0.219	0.00082
0.010	-0.959				
0.000	0.807				

TABLE 2-09

NACA 0020 AIRFOIL MODEL

M	REC	ALPHAC	CL(B)	CL(P)
0.297	19.8E06	8.75	0.868	0.858

Upper Surface			Lower Surface		
X/C	CP	CF	X/C	CP	CF
0.980	0.234	-.00004	0.020	0.986	
0.970	0.221	0.00011	0.040	0.768	
0.960	0.199		0.050	0.644	
0.950	0.192		0.060	0.555	
0.940	0.176		0.070	0.483	
0.930	0.157		0.080	0.422	
0.920	0.140		0.090	0.369	
0.910	0.114		0.100	0.307	
0.900	0.107		0.125	0.207	
0.880	0.066	0.00070	0.150	0.133	
0.860	0.028		0.175	0.063	
0.830	-0.029		0.200	0.018	
0.800	-0.084	0.00106	0.225	-0.009	
0.750	-0.178		0.250	-0.045	
0.700	-0.258	0.00144	0.275	-0.056	0.00480
0.600	-0.443		0.300	-0.072	
0.500	-0.648	0.00245	0.350	-0.107	0.00288
0.450	-0.751		0.400	-0.111	0.00293
0.400	-0.878	0.00316	0.450	-0.105	
0.350	-1.015	0.00351	0.500	-0.103	0.00264
0.300	-1.164		0.600	-0.074	
0.275	-1.240	0.00374	0.700	-0.051	0.00250
0.250	-1.326		0.750	-0.032	
0.225	-1.434		0.800	-0.008	0.00234
0.200	-1.543	0.00475	0.830	-0.003	
0.175	-1.653		0.860	0.017	
0.150	-1.776	0.00595	0.880	0.032	0.00217
0.125	-1.917		0.900	0.047	
0.100	-2.058		0.910	0.050	
0.090	-2.159		0.920	0.059	
0.080	-2.224		0.930	0.046	
0.070	-2.285		0.940	0.051	
0.060	-2.347		0.950	0.066	
0.050	-2.433		0.960	0.080	
0.040	-2.471		0.970	0.105	0.00167
0.030	-2.503		0.980	0.130	0.00150
0.020	-2.418				
0.010	-2.634				
0.000	0.067				
0.010	1.024				

TABLE 2-10

NACA 0020 AIRFOIL MODEL
(Trip Wires On)

M	REC	ALPHAC	CL(B)	CL(P)
0.299	5.0E06	0.03	-0.003	-0.011

Upper Surface			Lower Surface		
X/C	CP	CF	X/C	CP	CF
0.980	0.219	0.00039	0.000	1.051	
0.970	0.181	0.00055	0.010	0.167	
0.960	0.140		0.020	-0.097	
0.950	0.109		0.040	-0.351	
0.940	0.092		0.060	-0.499	
0.930	0.083		0.070	-0.581	
0.920	0.076		0.080	-0.639	
0.910	0.062		0.090	-0.679	
0.900	0.055		0.100	-0.700	
0.880	0.034		0.125	-0.721	
0.860	0.013	0.00142	0.150	-0.728	0.00559
0.830	-0.021		0.175	-0.726	
0.800	-0.063	0.00171	0.200	-0.712	0.00584
0.750	-0.124	0.00222	0.225	-0.686	
0.700	-0.181	0.00181	0.250	-0.663	
0.600	-0.291		0.275	-0.643	0.00467
0.500	-0.397	0.00316	0.300	-0.621	
0.450	-0.447		0.350	-0.598	0.00411
0.400	-0.509	0.00375	0.400	-0.547	0.00410
0.350	-0.585	0.00400	0.450	-0.488	
0.300	-0.642		0.500	-0.407	0.00327
0.275	-0.659	0.00480	0.600	-0.293	
0.250	-0.663		0.700	-0.189	0.00189
0.225	-0.679		0.750	-0.138	0.00235
0.200	-0.693	0.00568	0.800	-0.076	0.00185
0.175	-0.705		0.830	-0.037	
0.150	-0.717	0.00550	0.860	0.012	0.00143
0.125	-0.712		0.880	0.046	
0.100	-0.679		0.900	0.074	
0.090	-0.663		0.910	0.075	
0.080	-0.643		0.920	0.082	
0.070	-0.584		0.930	0.100	
0.060	-0.460		0.940	0.107	
0.040	-0.368		0.950	0.124	
0.030	-0.254		0.960	0.139	
0.020	-0.068		0.970	0.161	0.00078
0.010	0.207		0.980	0.196	0.00066

TABLE 2-11

NACA 0020 AIRFOIL MODEL
(Trip Wires On)

M	REC	ALPHAC	CL(B)	CL(P)
0.299	5.0E06	4.55	0.390	0.391

Upper Surface			Lower Surface		
X/C	CP	CF	X/C	CP	CF
0.980	0.229	0.00038	0.010	0.776	
0.970	0.224	-.00046	0.020	0.566	
0.960	0.216		0.040	0.282	
0.950	0.201		0.060	0.091	
0.940	0.180		0.070	-0.004	
0.930	0.165		0.080	-0.062	
0.920	0.147		0.090	-0.102	
0.910	0.128		0.100	-0.132	
0.900	0.107		0.125	-0.213	
0.880	0.073		0.150	-0.257	0.00435
0.860	0.030	0.00063	0.175	-0.298	
0.830	-0.029		0.200	-0.317	0.00487
0.800	-0.082	0.00157	0.225	-0.335	
0.750	-0.162	0.00184	0.250	-0.346	
0.700	-0.244	0.00191	0.275	-0.354	0.00425
0.600	-0.390		0.300	-0.353	
0.500	-0.545	0.00335	0.350	-0.346	0.00362
0.450	-0.628		0.400	-0.322	0.00395
0.400	-0.700	0.00376	0.450	-0.300	
0.350	-0.767	0.00360	0.500	-0.296	0.00346
0.300	-0.862		0.600	-0.244	
0.275	-0.913	0.00479	0.700	-0.177	0.00250
0.250	-0.970		0.750	-0.140	0.00303
0.225	-1.024		0.800	-0.097	0.00225
0.200	-1.072	0.00626	0.830	-0.063	
0.175	-1.125		0.860	-0.028	0.00225
0.150	-1.179	0.00644	0.880	-0.003	
0.125	-1.240		0.900	0.030	
0.100	-1.285		0.910	0.046	
0.090	-1.320		0.920	0.055	
0.080	-1.334		0.930	0.068	
0.070	-1.301		0.940	0.078	
0.060	-1.208		0.950	0.099	
0.040	-1.251		0.960	0.119	
0.030	-1.226		0.970	0.150	0.00127
0.020	-1.097		0.980	0.187	0.00065
0.010	-0.913				
0.000	0.819				

TABLE 2-12

NACA 0020 AIRFOIL MODEL
(Trip Wires On)

M	REC	ALPHAC	CL(B)	CL(P)
0.299	5.0E06	8.87	0.792	0.788

Upper Surface			Lower Surface		
X/C	CP	CF	X/C	CP	CF
0.980	0.141	-.00049	0.020	0.972	
0.970	0.135	0.00025	0.040	0.760	
0.960	0.137		0.060	0.562	
0.950	0.141		0.070	0.483	
0.940	0.133		0.080	0.417	
0.930	0.123		0.090	0.347	
0.920	0.122		0.100	0.291	
0.910	0.118		0.125	0.183	
0.900	0.105		0.150	0.103	0.00377
0.880	0.083		0.175	0.037	
0.860	0.049	-.00013	0.200	-0.006	0.00436
0.830	0.003		0.225	-0.037	
0.800	-0.046	0.00079	0.250	-0.072	
0.750	-0.140	0.00155	0.275	-0.090	0.00375
0.700	-0.234	0.00130	0.300	-0.107	
0.600	-0.417		0.350	-0.137	0.00340
0.500	-0.622	0.00286	0.400	-0.140	0.00394
0.450	-0.731		0.450	-0.139	
0.400	-0.845	0.00351	0.500	-0.141	0.00323
0.350	-0.974	0.00333	0.600	-0.119	
0.300	-1.117		0.700	-0.094	0.00265
0.275	-1.201	0.00480	0.750	-0.077	0.00298
0.250	-1.288		0.800	-0.062	0.00250
0.225	-1.386		0.830	-0.045	
0.200	-1.485	0.00717	0.860	-0.024	0.00251
0.175	-1.587		0.880	-0.016	
0.150	-1.715	0.00761	0.900	0.000	
0.125	-1.851		0.910	0.008	
0.100	-1.986		0.920	0.014	
0.090	-2.050		0.930	0.013	
0.080	-2.090		0.940	0.002	
0.070	-2.126		0.950	0.011	
0.060	-2.151		0.960	0.023	
0.040	-2.320		0.970	0.041	0.00164
0.030	-2.417		0.980	0.065	0.00200
0.020	-2.465				
0.010	-2.484				
0.000	0.157				
0.010	1.037				

TABLE 2-13

SUPERCRITICAL AIRFOIL MODEL

M	REC	ALPHAC	CL(B)	CL(P)
0.740	15.2E06	-0.09	0.024	0.021

Upper Surface			Lower Surface		
X/C	CP	CF	X/C	CP	CF
1.000	0.235		0.000	1.142	
0.978	0.217	0.00004	0.002	0.871	
0.956	0.192	0.00017	0.008	0.360	
0.934	0.163	0.00022	0.016	-0.062	
0.913	0.134		0.024	-0.270	
0.892	0.099		0.042	-0.310	
0.871	0.045	0.00034	0.077	-0.370	
0.849	-0.038		0.112	-0.453	0.00408
0.829	-0.133		0.148	-0.499	
0.809	-0.244	0.00111	0.185	-0.535	
0.788	-0.334		0.223	-0.580	0.00322
0.765	-0.408		0.268	-0.625	
0.741	-0.464		0.308	-0.621	
0.722	-0.515		0.346	-0.634	
0.703	-0.551	0.00248	0.384	-0.655	0.00294
0.684	-0.562		0.422	-0.654	
0.664	-0.555		0.462	-0.640	
0.644	-0.547		0.502	-0.652	
0.624	-0.544	0.00241	0.542	-0.638	0.00242
0.604	-0.524		0.582	-0.632	
0.584	-0.505		0.623	-0.622	
0.564	-0.501	0.00232	0.663	-0.584	0.00208
0.538	-0.470		0.702	-0.424	
0.513	-0.515	0.00249	0.742	-0.243	0.00112
0.488	-0.517		0.780	-0.051	
0.462	-0.557		0.823	0.062	0.00015
0.436	-0.596	0.00258	0.865	0.121	0.00010
0.409	-0.602		0.908	0.171	0.00007
0.384	-0.595		0.952	0.217	
0.357	-0.609	0.00310	1.000	0.235	
0.331	-0.601				
0.306	-0.593				
0.279	-0.607				
0.254	-0.620	0.00312			
0.227	-0.637				
0.202	-0.652				
0.176	-0.656	0.00401			
0.150	-0.615				
0.125	-0.576				
0.105	-0.525				
0.091	-0.474				
0.081	-0.421				
0.071	-0.386				
0.061	-0.362				
0.052	-0.317				
0.043	-0.246				
0.033	-0.164				
0.024	-0.020				
0.016	0.173				
0.008	0.464				
0.003	0.910				

TABLE 2-14

SUPERCRITICAL AIRFOIL MODEL

M	REC	ALPHAC	CL(B)	CL(P)
0.740	15.2E06	1.18	0.241	0.234

Upper Surface			Lower Surface		
X/C	CP	CF	X/C	CP	CF
1.000	0.216		0.002	1.013	
0.978	0.205	0.00007	0.008	0.610	
0.956	0.185	0.00009	0.016	0.239	
0.934	0.158	0.00017	0.024	0.040	
0.913	0.132		0.042	-0.041	
0.892	0.099		0.077	-0.136	
0.871	0.045	0.00040	0.112	-0.231	0.00364
0.849	-0.026		0.143	-0.293	
0.829	-0.121		0.185	-0.345	
0.809	-0.235	0.00114	0.223	-0.401	0.00304
0.788	-0.327		0.268	-0.455	
0.765	-0.395		0.308	-0.464	
0.741	-0.456		0.346	-0.487	
0.722	-0.511		0.384	-0.521	0.00296
0.703	-0.555	0.00248	0.422	-0.521	
0.684	-0.567		0.462	-0.528	
0.664	-0.567		0.502	-0.547	
0.644	-0.568		0.542	-0.552	0.00247
0.624	-0.571	0.00244	0.582	-0.567	
0.604	-0.555		0.623	-0.573	
0.584	-0.545		0.663	-0.559	0.00217
0.564	-0.539	0.00233	0.702	-0.424	
0.538	-0.518		0.742	-0.255	0.00133
0.513	-0.560	0.00239	0.780	-0.062	
0.488	-0.572		0.823	0.085	0.00026
0.462	-0.619		0.865	0.161	0.00017
0.436	-0.659	0.00239	0.908	0.220	0.00014
0.409	-0.652		0.952	0.260	
0.384	-0.624		1.000	0.216	
0.357	-0.627	0.00219			
0.331	-0.892				
0.306	-0.930				
0.279	-0.943				
0.254	-0.950	0.00356			
0.227	-0.954				
0.202	-0.946				
0.176	-0.923	0.00431			
0.150	-0.864				
0 125	-0.803				
0.105	-0.759				
0.091	-0.715				
0.081	-0.665				
0.071	-0.621				
0.061	-0.613				
0.052	-0.591				
0.043	-0.518				
0.033	-0.438				
0.024	-0.275				
0.016	-0.095				
0.008	0.203				
0.003	0.731				
0.000	1.123				

TABLE 2-15

SUPERCRITICAL AIRFOIL MODEL

M	REC	ALPHAC	CL(B)	CL(P)
0.740	15.2E06	2.38	0.505	0.504

Upper Surface			Lower Surface		
X/C	CP	CF	X/C	CP	CF
1.000	0.255		0.002	1.110	
0.978	0.236	0.00012	0.008	0.807	
0.956	0.209	0.00034	0.016	0.505	
0.934	0.183	0.00030	0.024	0.319	
0.913	0.148		0.042	0.189	
0.892	0.095		0.077	0.065	
0.871	0.025	0.00068	0.112	-0.043	
0.849	-0.051		0.148	-0.111	
0.829	-0.148		0.185	-0.175	
0.809	-0.249	0.00131	0.223	-0.236	
0.788	-0.326		0.268	-0.291	
0.765	-0.394		0.308	-0.311	
0.741	-0.439		0.346	-0.337	
0.722	-0.478		0.384	-0.375	
0.703	-0.508	0.00232	0.422	-0.380	
0.684	-0.517		0.462	-0.398	
0.664	-0.512		0.502	-0.423	
0.644	-0.498		0.542	-0.434	0.00239
0.624	-0.481	0.00178	0.582	-0.452	
0.604	-0.469		0.623	-0.471	
0.584	-0.452		0.663	-0.482	0.00226
0.564	-0.454	0.00087	0.702	-0.375	
0.538	-0.470		0.742	-0.218	0.00146
0.513	-0.536	0.00045	0.780	-0.034	
0.488	-0.736		0.823	0.125	0.00039
0.462	-1.198		0.865	0.216	0.00014
0.436	-1.236	0.00304	0.908	0.272	0.00017
0.409	-1.222		0.952	0.310	
0.384	-1.213		1.000	0.255	
0.357	-1.227	0.00337			
0.331	-1.212				
0.306	-1.200				
0.279	-1.195				
0.254	-1.186	0.00365			
0.227	-1.177				
0.202	-1.160				
0.176	-1.132	0.00426			
0.150	-1.088				
0.125	-1.038				
0.105	-0.985	0.00525			
0.091	-0.935				
0.081	-0.885				
0.071	-0.869				
0.061	-0.910				
0.052	-0.898				
0.043	-0.816				
0.033	-0.730				
0.024	-0.556				
0.016	-0.380				
0.008	-0.097				
0.003	0.497				
0.000	1.047				

TABLE 2-16

SUPERCRITICAL AIRFOIL MODEL

M	REC	ALPHAC	CL(B)	CL(P)
0.740	15.2E06	3.67	0.697	0.691

Upper Surface			Lower Surface		
X/C	CP	CF	X/C	CP	CF
1.000	0.208		0.002	1.143	
0.978	0.200	0.00024	0.008	0.949	
0.956	0.173	0.00022	0.016	0.679	
0.934	0.150	0.00023	0.024	0.500	
0.913	0.115		0.042	0.366	
0.892	0.077		0.077	0.211	
0.871	0.032	0.00037	0.112	0.094	
0.849	-0.027		0.148	0.019	
0.829	-0.092		0.185	-0.044	
0.809	-0.157	0.00083	0.223	-0.113	0.00269
0.788	-0.216		0.268	-0.178	
0.765	-0.262		0.308	-0.203	
0.741	-0.300		0.346	-0.234	
0.722	-0.334		0.384	-0.275	
0.703	-0.360	0.00091	0.422	-0.294	
0.684	-0.383		0.462	-0.318	
0.664	-0.422		0.502	-0.347	
0.644	-0.485		0.542	-0.375	0.00245
0.624	-0.535	-0.00003	0.582	-0.398	
0.604	-0.601		0.623	-0.427	
0.584	-0.668		0.663	-0.449	0.00233
0.564	-0.724	-0.00005	0.702	-0.358	
0.538	-0.770		0.742	-0.221	0.00164
0.513	-0.889	0.00036	0.780	-0.039	
0.488	-1.391		0.823	0.127	0.00053
0.462	-1.446		0.865	0.227	0.00030
0.436	-1.439	0.00304	0.908	0.292	0.00023
0.409	-1.414		0.952	0.314	
0.384	-1.392		1.000	0.208	
0.357	-1.402	0.00326			
0.331	-1.388				
0.306	-1.369				
0.279	-1.358				
0.254	-1.353	0.00358			
0.227	-1.349				
0.202	-1.335				
0.176	-1.308	0.00422			
0.150	-1.262				
0.125	-1.223				
0.105	-1.193				
0.091	-1.170				
0.081	-1.135				
0.071	-1.097				
0.061	-1.147				
0.052	-1.114				
0.043	-1.023				
0.033	-0.921				
0.024	-0.780				
0.016	-0.626				
0.008	-0.336				
0.003	0.276				
0.000	0.939				

TABLE 2-17

SUPERCRITICAL AIRFOIL MODEL

M	REC	ALPHAC	CL(B)	CL(P)
0.739	19.8E06	-0.13	0.031	0.035

Upper Surface			Lower Surface		
X/C	CP	CF	X/C	CP	CF
1.000	0.250		0.000	1.145	
0.978	0.228	0.00008	0.002	0.878	
0.956	0.201	0.00023	0.008	0.363	
0.934	0.173	0.00026	0.016	-0.046	
0.913	0.140		0.024	-0.227	
0.892	0.100		0.042	-0.305	
0.871	0.037	0.00037	0.077	-0.348	
0.849	-0.051		0.112	-0.430	
0.829	-0.155		0.148	-0.476	
0.809	-0.269	0.00117	0.185	-0.518	0.00303
0.788	-0.356		0.223	-0.552	0.00291
0.765	-0.418		0.268	-0.613	
0.741	-0.470		0.308	-0.615	0.00290
0.722	-0.522		0.346	-0.621	
0.703	-0.558	0.00235	0.384	-0.635	0.00273
0.684	-0.569		0.422	-0.639	
0.664	-0.561		0.462	-0.628	
0.644	-0.551		0.502	-0.635	
0.624	-0.541	0.00226	0.542	-0.629	0.00224
0.604	-0.529		0.582	-0.629	
0.584	-0.514		0.623	-0.618	
0.564	-0.500	0.00216	0.663	-0.572	0.00195
0.538	-0.461		0.702	-0.425	
0.513	-0.504	0.00232	0.742	-0.239	0.00102
0.488	-0.509		0.780	-0.049	
0.462	-0.548		0.823	0.085	0.00003
0.436	-0.582	0.00227	0.865	0.154	-0.00006
0.409	-0.590		0.908	0.200	0.00001
0.384	-0.593		0.952	0.246	
0.357	-0.607	0.00286	1.000	0.250	
0.331	-0.599				
0.306	-0.597				
0.279	-0.604				
0.254	-0.606	0.00283			
0.227	-0.623				
0.202	-0.642				
0.176	-0.653	0.00366			
0.150	-0.610				
0.125	-0.576				
0.105	-0.520				
0.091	-0.479				
0.081	-0.431				
0.071	-0.385				
0.061	-0.340				
0.052	-0.297				
0.043	-0.246				
0.033	-0.146				
0.024	0.014				
0.016	0.182				
0.008	0.466				
0.003	0.901				

TABLE 2-18

SUPERCRITICAL AIRFOIL MODEL

M	REC	ALPHAC	CL(B)	CL(P)
0.739	19.8E06	1.16	0.247	0.245

Upper Surface			Lower Surface		
X/C	CP	CF	X/C	CP	CF
1.000	0.233		0.002	1.040	
0.978	0.218	0.00010	0.008	0.628	
0.956	0.190	0.00022	0.016	0.266	
0.934	0.167	0.00022	0.024	0.078	
0.913	0.135		0.042	-0.027	
0.892	0.092		0.077	-0.131	
0.871	0.031	0.00051	0.112	-0.223	
0.849	-0.035		0.148	-0.288	
0.829	-0.130		0.185	-0.335	0.00292
0.809	-0.242	0.00109	0.223	-0.375	0.00273
0.788	-0.334		0.268	-0.443	0.00278
0.765	-0.405		0.308	-0.464	
0.741	-0.465		0.346	-0.478	
0.722	-0.523		0.384	-0.506	0.00272
0.703	-0.566	0.00223	0.422	-0.512	
0.684	-0.581		0.462	-0.521	
0.664	-0.577		0.502	-0.540	
0.644	-0.564		0.542	-0.549	0.00237
0.624	-0.563	0.00215	0.582	-0.553	
0.604	-0.563		0.623	-0.563	
0.584	-0.546		0.663	-0.544	0.00213
0.564	-0.538	0.00216	0.702	-0.520	
0.538	-0.506		0.742	-0.251	0.00130
0.513	-0.556	0.00224	0.780	-0.056	
0.488	-0.567		0.823	0.096	0.00028
0.462	-0.613		0.865	0.185	0.00009
0.436	-0.661	0.00229	0.908	0.243	0.00013
0.409	-0.672		0.952	0.286	
0.384	-0.635		1.000	0.233	
0.357	-0.618	0.00199			
0.331	-0.842				
0.306	-0.922				
0.279	-0.932				
0.254	-0.941	0.00326			
0.227	-0.952				
0.202	-0.946				
0.176	-0.918	0.00395			
0.150	-0.863				
0.125	-0.811				
0.105	-0.755				
0.091	-0.716				
0.081	-0.675				
0.071	-0.620				
0.061	-0.584				
0.052	-0.573				
0.043	-0.527				
0.033	-0.416				
0.024	-0.249				
0.016	-0.077				
0.008	0.228				
0.003	0.729				
0.000	1.131				

TABLE 2-19

SUPERCRITICAL AIRFOIL MODEL

M	REC	ALPHAC	CL(B)	CL(P)
0.739	19.8E06	2.37	0.504	0.496

Upper Surface			Lower Surface		
X/C	CP	CF	X/C	CP	CF
1.000	0.264		0.002	1.116	
0.978	0.239	0.00017	0.008	0.828	
0.956	0.214	0.00032	0.016	0.513	
0.934	0.181	0.00039	0.024	0.341	
0.913	0.142		0.042	0.197	
0.892	0.090		0.077	0.073	
0.871	0.022	0.00068	0.112	-0.034	
0.849	-0.058		0.148	-0.109	
0.829	-0.155		0.185	-0.170	0.00280
0.809	-0.263	0.00127	0.223	-0.222	0.00264
0.788	-0.338		0.268	-0.281	0.00264
0.765	-0.404		0.308	-0.317	
0.741	-0.450		0.346	-0.339	
0.722	-0.495		0.384	-0.366	0.00257
0.703	-0.522	0.00213	0.422	-0.381	
0.684	-0.524		0.462	-0.398	
0.664	-0.516		0.502	-0.425	
0.644	-0.500		0.542	-0.441	0.00235
0.624	-0.493	0.00159	0.582	-0.457	
0.604	-0.475		0.623	-0.475	
0.584	-0.457		0.663	-0.471	0.00212
0.564	-0.447	0.00093	0.702	-0.376	
0.538	-0.436		0.742	-0.230	0.00148
0.513	-0.511	0.00032	0.780	-0.036	
0.488	-0.615		0.823	0.131	0.00036
0.462	-0.988		0.865	0.224	0.00017
0.436	-1.224	0.00272	0.908	0.284	0.00024
0.409	-1.217		0.952	0.315	
0.384	-1.203		1.000	0.264	
0.357	-1.214	0.00311			
0.331	-1.201				
0.306	-1.197				
0.279	-1.190				
0.254	-1.184	0.00341			
0.227	-1.175				
0.202	-1.155				
0.176	-1.122	0.00384			
0.150	-1.080				
0.125	-1.030				
0.105	-0.976	0.00473			
0.091	-0.934				
0.081	-0.904				
0.071	-0.869				
0.061	-0.860				
0.052	-0.877				
0.043	-0.822				
0.033	-0.712				
0.024	-0.554				
0.016	-0.362				
0.008	-0.061				
0.003	0.480				
0.000	1.038				

TABLE 2-20

SUPERCRITICAL AIRFOIL MODEL

M	REC	ALPHAC	CL(B)	CL(P)
0.739	19.8E06	3.67	0.700	0.689

Upper Surface			Lower Surface		
X/C	CP	CF	X/C	CP	CF
1.000	0.233		0.002	1.140	
0.978	0.216	0.00013	0.008	0.952	
0.956	0.188	0.00027	0.016	0.682	
0.934	0.161	0.00014	0.024	0.521	
0.913	0.127		0.042	0.375	
0.892	0.085		0.077	0.217	
0.871	0.037	0.00084	0.112	0.101	
0.849	-0.023		0.148	0.021	
0.829	-0.094		0.185	-0.040	
0.809	-0.167	0.00085	0.223	-0.100	0.00251
0.788	-0.227		0.268	-0.167	0.00255
0.765	-0.265		0.308	-0.193	
0.741	-0.313		0.346	-0.231	
0.722	-0 335		0.384	-0.263	0.00252
0.703	-0.357	0.00097	0.422	-0.288	
0.684	-0.376		0.462	-0.313	
0.664	-0.403		0.502	-0.342	
0.644	-0.451		0.542	-0.367	0.00229
0.624	-0.501	-.00005	0.582	-0.390	
0.604	-0.561		0.623	-0.413	
0.584	-0.625		0.663	-0.425	0.00216
0.564	-0.695	-.00016	0.702	-0.350	
0.538	-0.735		0.742	-0.209	0.00157
0.513	-0.872	0.00027	0.780	-0.031	
0.486	-1.368		0.823	0.141	0.00045
0.462	-1.436		0.865	0.241	0.00028
0.436	-1.429	0.00281	0.908	0.305	0.00028
0.409	-1.407		0.952	0.323	
0.384	-1.384		1.000	0.233	
0.357	-1.395	0.00293			
0.331	-1.381				
0.306	-1.365				
0.279	-1.350				
0.254	-1.338	0.00324			
0.227	-1.331				
0.202	-1.323				
0.176	-1.298	0.00384			
0.150	-1.249				
0.125	-1.207				
0.105	-1.177	0.00469			
0.091	-1.164				
0.081	-1.139				
0.071	-1.089				
0.061	-1.115				
0.052	-1.107				
0.043	-1.019				
0.033	-0.905				
0.024	-0.771				
0.016	-0.581				
0.008	-0.280				
0.003	0.285				
0.000	0.937				

TABLE 2-21

SUPERCRITICAL AIRFOIL MODEL

M	REC	ALPHAC	CL(B)	CL(P)
0.739	24.9E06	-0.15	0.038	0.040

Upper Surface			Lower Surface		
X/C	CP	CF	X/C	CP	CF
1.000	0.252		0.000	1.144	
0.978	0.229	0.00003	0.002	0.879	
0.956	0.204	0.00018	0.008	0.365	
0.934	0.178	0.00021	0.016	-0.065	
0.913	0.140		0.024	-0.257	
0.892	0.088		0.042	-0.318	
0.871	0.019	0.00053	0.077	-0.360	
0.849	-0.064		0.112	-0.436	0.00497
0.829	-0.166		0.148	-0.492	
0.809	-0.288	0.00128	0.185	-0.537	
0.788	-0.378		0.223	-0.568	0.00284
0.765	-0.445		0.268	-0.635	
0.741	-0.487		0.308	-0.633	
0.722	-0.546		0.346	-0.641	
0.703	-0.581		0.384	-0.670	0.00256
0.684	-0.589		0.422	-0.663	
0.664	-0.580		0.462	-0.654	
0.644	-0.567		0.502	-0.660	
0.624	-0.558	0.00220	0.542	-0.643	0.00337
0.604	-0.550		0.582	-0.639	
0.584	-0.537		0.623	-0.631	
0.564	-0.516	0.00210	0.663	-0.581	0.00188
0.538	-0.481		0.702	-0.433	
0.513	-0.526	0.00231	0.742	-0.257	0.00171
0.488	-0.528		0.780	-0.064	
0.462	-0.561		0.823	0.083	0.00016
0.436	-0.603	0.00231	0.865	0.160	0.00010
0.409	-0.627		0.908	0.212	-.00014
0.384	-0.619		0.952	0.256	
0.357	-0.630	0.00276	1.000	0.252	
0.331	-0.621				
0.306	-0.616				
0.279	-0.625				
0.254	-0.630	0.00276			
0.227	-0.648				
0.202	-0.668				
0.176	-0.677	0.00356			
0.150	-0.637				
0.125	-0.593				
0.105	-0.530				
0.091	-0.483				
0.081	-0.446				
0.071	-0.406				
0.061	-0.377				
0.052	-0.310				
0.043	-0.275				
0.033	-0.151				
0.024	-0.001				
0.016	0.160				
0.008	0.463				
0.003	0.905				

TABLE 2-22

SUPERCRITICAL AIRFOIL MODEL

M	REC	ALPHAC	CL(B)	CL(P)
0.739	24.9E06	1.15	0.262	0.261

Upper Surface

X/C	CP	CF
1.000	0.247	
0.978	0.221	0.00007
0.956	0.194	0.00020
0.934	0.172	0.00016
0.913	0.139	
0.892	0.097	
0.871	0.039	0.00038
0.849	-0.041	
0.829	-0.150	
0.809	-0.265	0.00111
0.788	-0.350	
0.765	-0.425	
0.741	-0.480	
0.722	-0.538	
0.703	-0.584	
0.684	-0.597	
0.664	-0.595	
0.644	-0.590	
0.624	-0.585	0.00216
0.604	-0.580	
0.584	-0.564	
0.564	-0.548	0.00214
0.538	-0.522	
0.513	-0.568	0.00214
0.488	-0.582	
0.462	-0.620	
0.436	-0.653	0.00214
0.409	-0.604	
0.384	-0.598	
0.357	-0.873	0.00272
0.331	-0.946	
0.306	-0.957	
0.279	-0.953	
0.254	-0.957	0.00313
0.227	-0.968	
0.202	-0.962	
0.176	-0.929	0.00370
0.150	-0.878	
0.125	-0.824	
0.105	-0.779	0.00424
0.091	-0.746	
0.081	-0.693	
0.071	-0.645	
0.061	-0.629	
0.052	-0.580	
0.043	-0.554	
0.033	-0.447	
0.024	-0.284	
0.016	-0.109	
0.008	0.214	
0.003	0.717	
0.000	1.119	

Lower Surface

X/C	CP	CF
0.002	1.020	
0.008	0.615	
0.016	0.256	
0.024	0.070	
0.042	-0.043	
0.077	-0.133	
0.112	-0.233	
0.148	-0.294	
0.185	-0.339	
0.223	-0.386	0.00271
0.268	-0.457	
0.308	-0.468	
0.346	-0.488	
0.384	-0.523	0.00258
0.422	-0.517	
0.462	-0.522	
0.502	-0.542	
0.542	-0.547	0.00230
0.582	-0.567	
0.623	-0.566	
0.663	-0.544	0.00201
0.702	-0.423	
0.742	-0.254	0.00132
0.780	-0.062	
0.823	0.104	0.00026
0.865	0.195	0.00015
0.908	0.258	0.00003
0.952	0.289	
1.000	0.247	

TABLE 2-23

SUPERCRITICAL AIRFOIL MODEL

M	REC	ALPHAC	CL(B)	CL(P)
0.739	24.9E06	2.39	0.520	0.512

Upper Surface			Lower Surface		
X/C	CP	CF	X/C	CP	CF
1.000	0.271		0.002	1.115	
0.978	0.247	-.00004	0.008	0.814	
0.956	0.216	0.00029	0.016	0.510	
0.934	0.185	0.00028	0.024	0.331	
0.913	0.150		0.042	0.197	
0.892	0.098		0.077	0.073	
0.871	0.022	0.00060	0.112	-0.040	
0.849	-0.063		0.148	-0.112	
0.829	-0.159		0.185	-0.173	
0.809	-0.268	0.0124	0.223	-0.228	0.00256
0.788	-0.349		0.268	-0.291	
0.765	-0.412		0.308	-0.313	
0.741	-0.448		0.346	-0.339	
0.722	-0.491		0.384	-0.378	0.00241
0.703	-0.513		0.422	-0.379	
0.684	-0.519		0.462	-0.396	
0.664	-0.502		0.502	-0.419	
0.644	-0.485		0.542	-0.437	0.00220
0.624	-0.473	0.00141	0.582	-0.459	
0.604	-0.459		0.623	-0.478	
0.584	-0.446		0.663	-0.473	0.00201
0.564	-0.444	0.00078	0.702	-0.373	
0.538	-0.461		0.742	-0.226	0.00142
0.513	-0.547	0.00018	0.780	-0.040	
0.488	-0.713		0.823	0.135	0.00045
0.462	-1.248		0.865	0.235	0.00021
0.436	-1.245	0.00271	0.908	0.298	0.00012
0.409	-1.224		0.952	0.323	
0.384	-1.216		1.000	0.271	
0.357	-1.233	0.00305			
0.331	-1.219				
0.306	-1.207				
0.279	-1.205				
0.254	-1.199	0.00323			
0.227	-1.186				
0.202	-1.165				
0.176	-1.134	0.00367			
0.150	-1.100				
0.125	-1.040				
0.105	-0.975	0.00427			
0.091	-0.928				
0.081	-0.909				
0.071	-0.900	0.00497			
0.061	-0.919				
0.052	-0.889				
0.043	-0.830				
0.033	-0.695				
0.024	-0.544				
0.016	-0.372				
0.008	-0.055				
0.003	0.493				
0.000	1.048				

TABLE 2-24

SUPERCRITICAL AIRFOIL MODEL

M	REC	ALPHAC	CL(B)	CL(P)
0.739	24.9E06	3.70	0.708	0.697

Upper Surface			Lower Surface		
X/C	CP	CF	X/C	CP	CF
1.000	0.237		0.002	1.143	
0.978	0.213	-.00002	0.008	0.944	
0.956	0.190	0.00022	0.016	0.673	
0.934	0.164	0.00026	0.024	0.518	
0.913	0.133		0.042	0.366	
0.892	0.086		0.077	0.221	
0.871	0.028	0.00058	0.112	0.102	
0.849	-0.030		0.148	0.018	
0.829	-0.101		0.185	-0.048	
0.809	-0.176	0.00104	0.223	-0.104	0.00246
0.788	-0.241		0.268	-0.178	
0.765	-0.286		0.308	-0.200	
0.741	-0.312		0.346	-0.235	
0.722	-0.338		0.384	-0.284	0.00237
0.703	-0.368		0.422	-0.294	
0.684	-0.382		0.462	-0.313	
0.664	-0.402		0.502	-0.346	
0.644	-0.437		0.542	-0.372	0.00221
0.624	-0.507	0.00012	0.582	-0.399	
0.604	-0.568		0.623	-0.423	0.00213
0.584	-0.631		0.663	-0.440	
0.564	-0.700	-.00012	0.702	-0.361	
0.538	-0.766		0.742	-0.219	0.00158
0.513	-1.014	0.00100	0.780	-0.039	
0.488	-1.436		0.823	0.142	0.00050
0.462	-1.439		0.865	0.244	0.00041
0.436	-1.431	0.00269	0.908	0.311	0.00032
0.409	-1.409		0.952	0.322	
0.384	-1.390		1.000	0.237	
0.357	-1.400	0.00285			
0.331	-1.385				
0.306	-1.371				
0.279	-1.364				
0.254	-1.350	0.00309			
0.227	-1.340				
0.202	-1.329				
0.176	-1.303	0.00360			
0.150	-1.263				
0.125	-1.223				
0.105	-1.183	0.00407			
0.091	-1.181				
0.081	-1.152				
0.071	-1.118	0.00493			
0.061	-1.165				
0.052	-1.112				
0.043	-1.040				
0.033	-0.915				
0.024	-0.783				
0.016	-0.609				
0.008	-0.299				
0.003	0.270				
0.000	0.943				

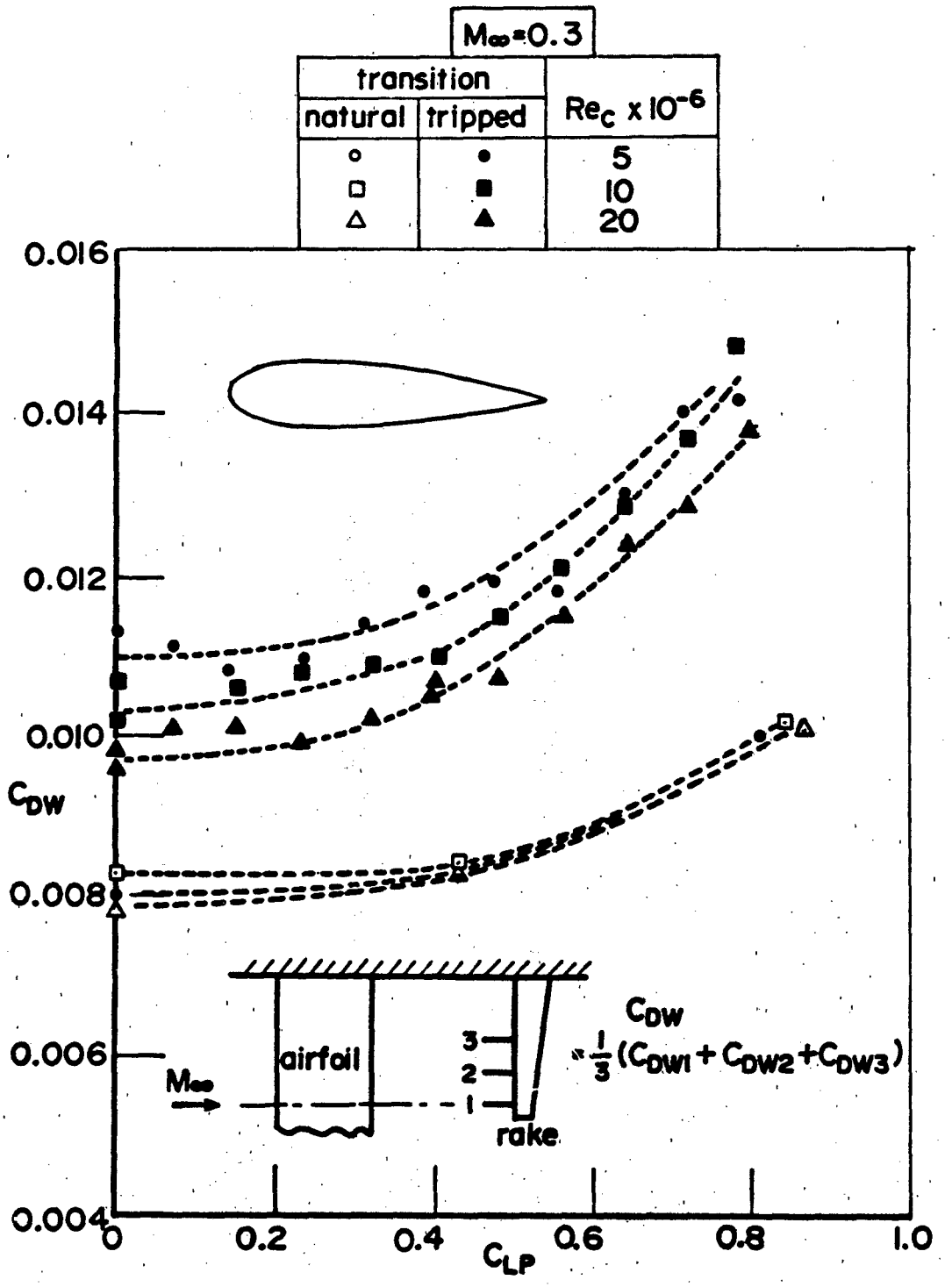

FIG. 1: INFLUENCE OF Re_c ON DRAG — NACA 0020 AIRFOIL

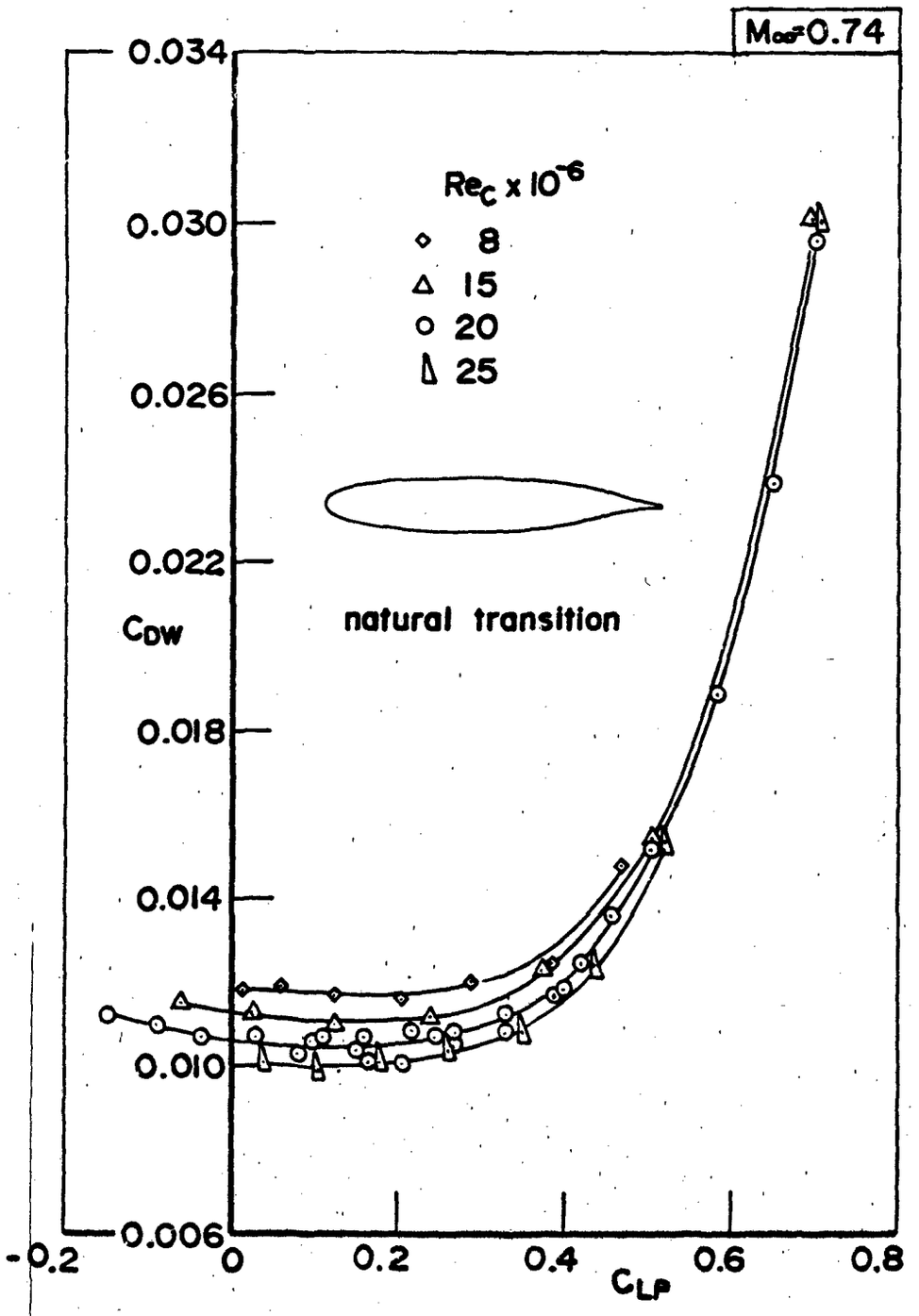

FIG. 2: INFLUENCE OF Re_c ON DRAG — 16% SUPERCRITICAL AIRFOIL

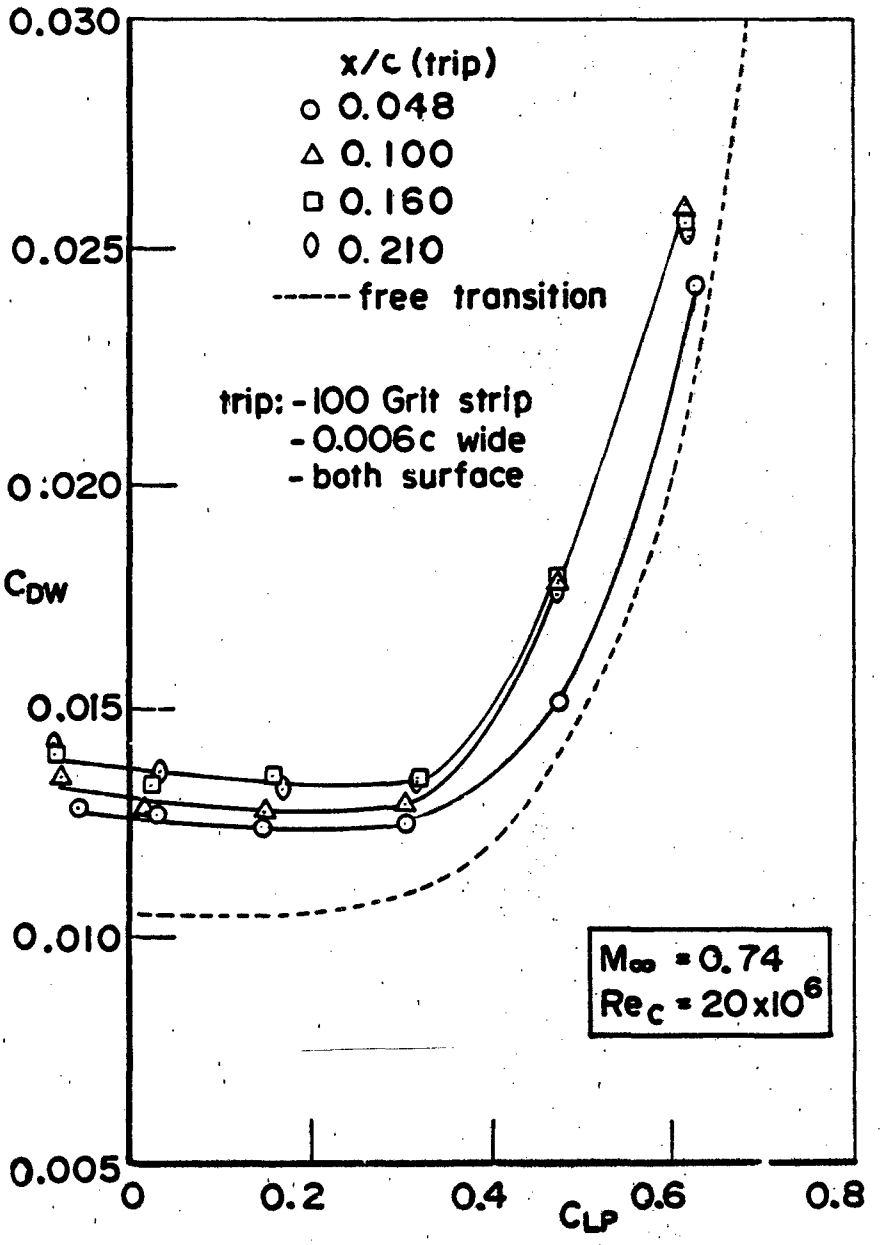

FIG. 3: INFLUENCE OF TRIP STRIP ON DRAG – SUPERCRITICAL AIRFOIL MODEL

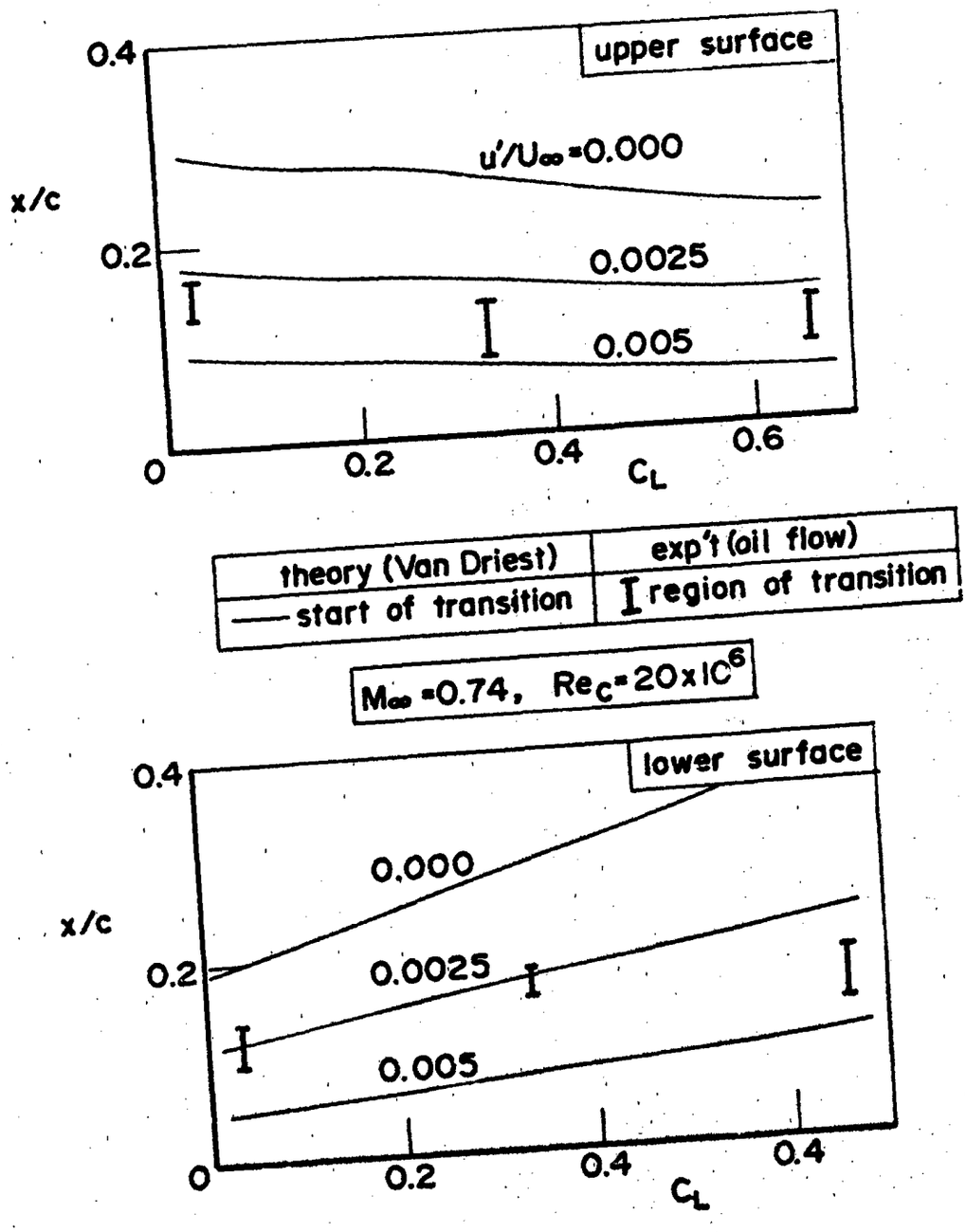

FIG. 4: TRANSITION -- SUPERCRITICAL AIRFOIL MODEL

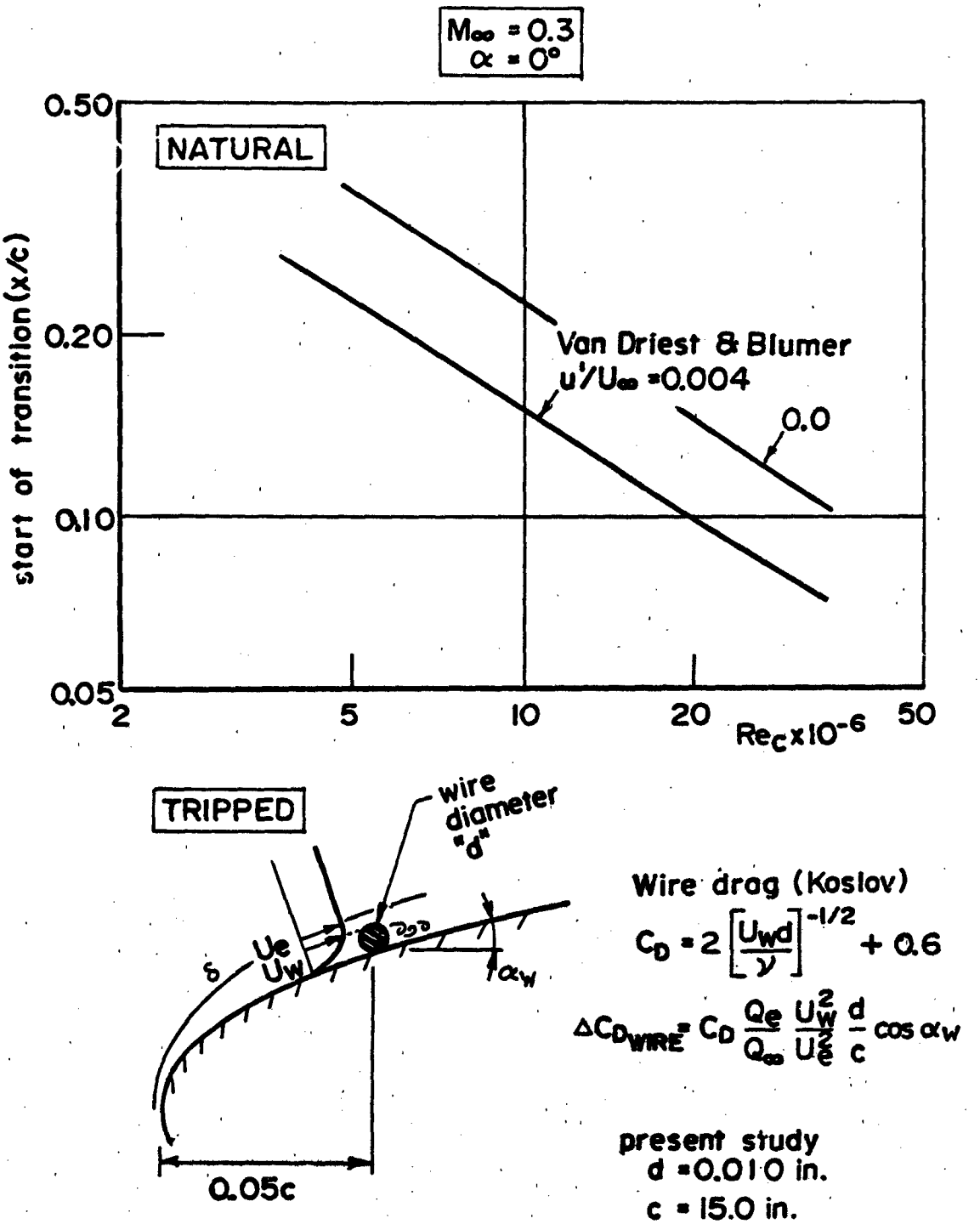

FIG. 5: TRANSITION — NACA 0020 AIRFOIL MODEL

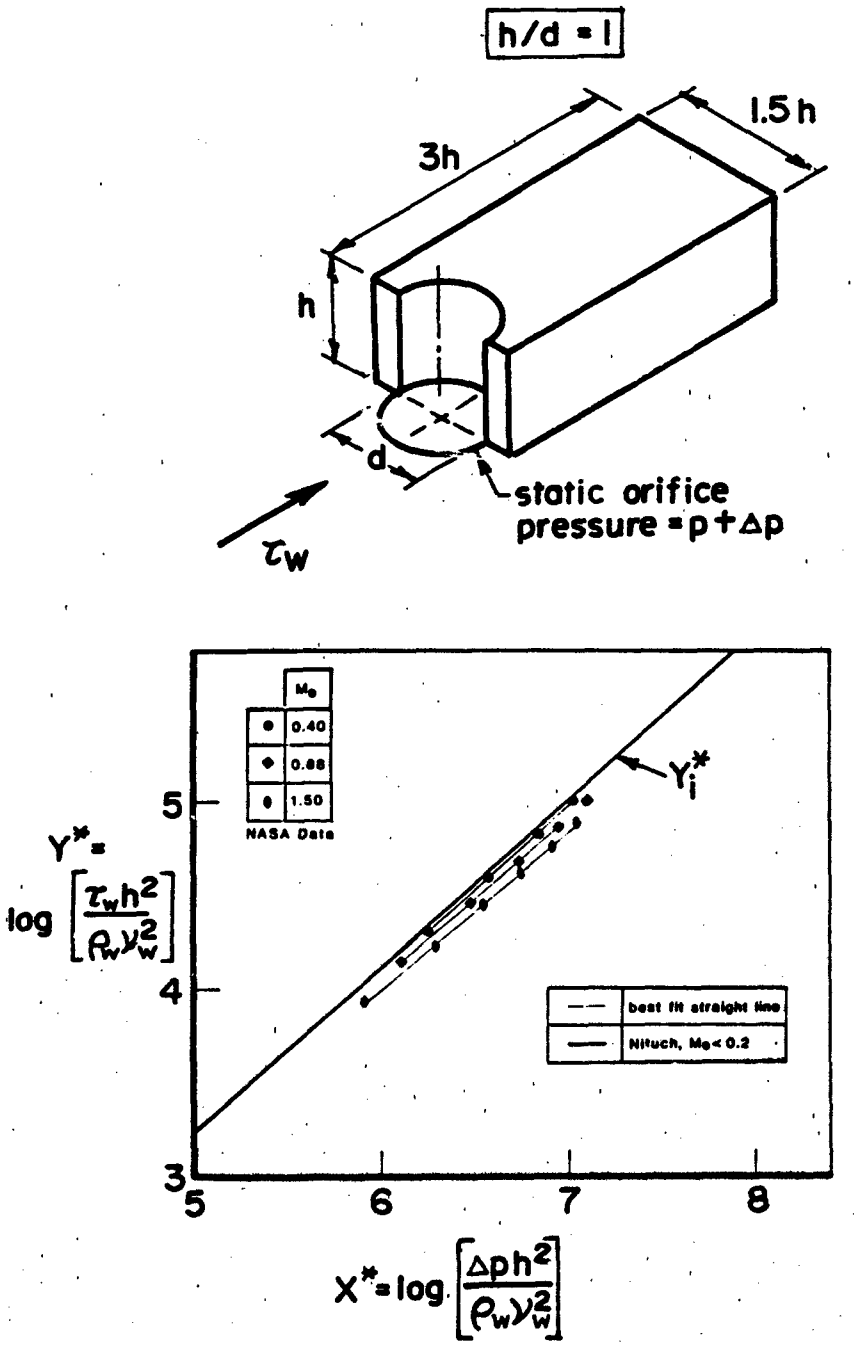

FIG. 6: THE CONGRUENT OBSTACLE BLOCK AS A SKIN FRICTION INDICATOR

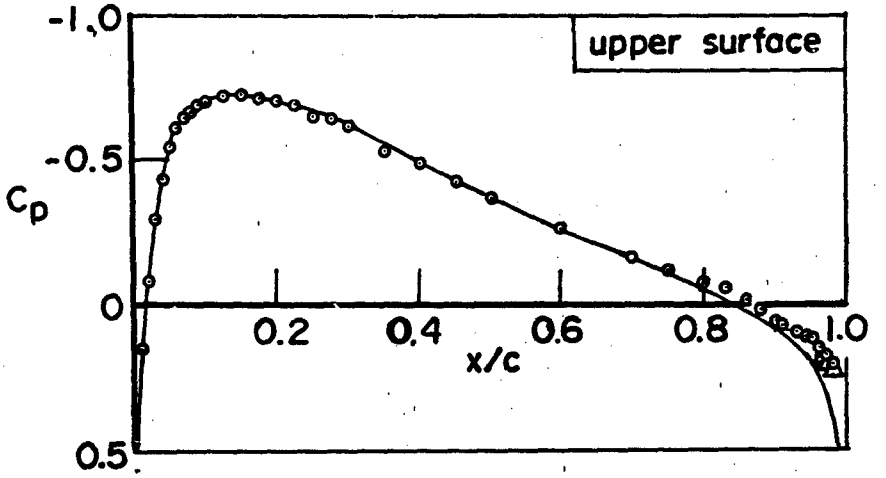

potential flow	exp't	Re_c x 10^{-6}
———	○	5
	△	20

$M_\infty = 0.3, \alpha = 0°$

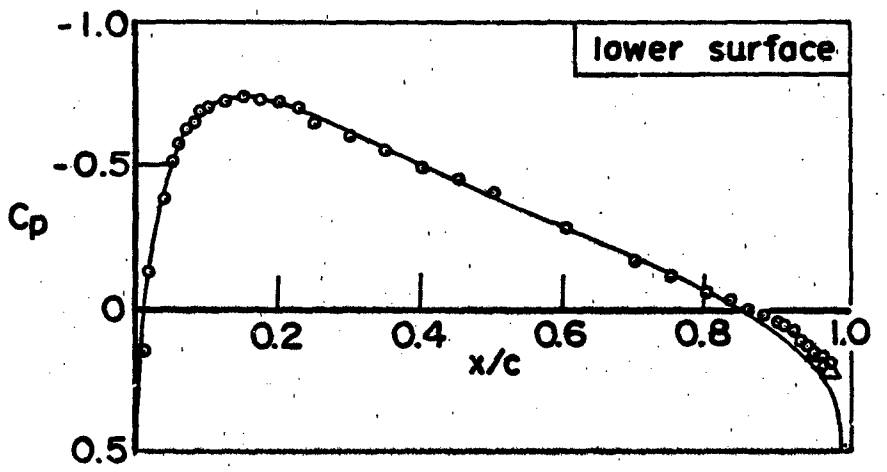

FIG. 7(a): C_p DISTRIBUTION – NACA 0020 AIRFOIL MODEL

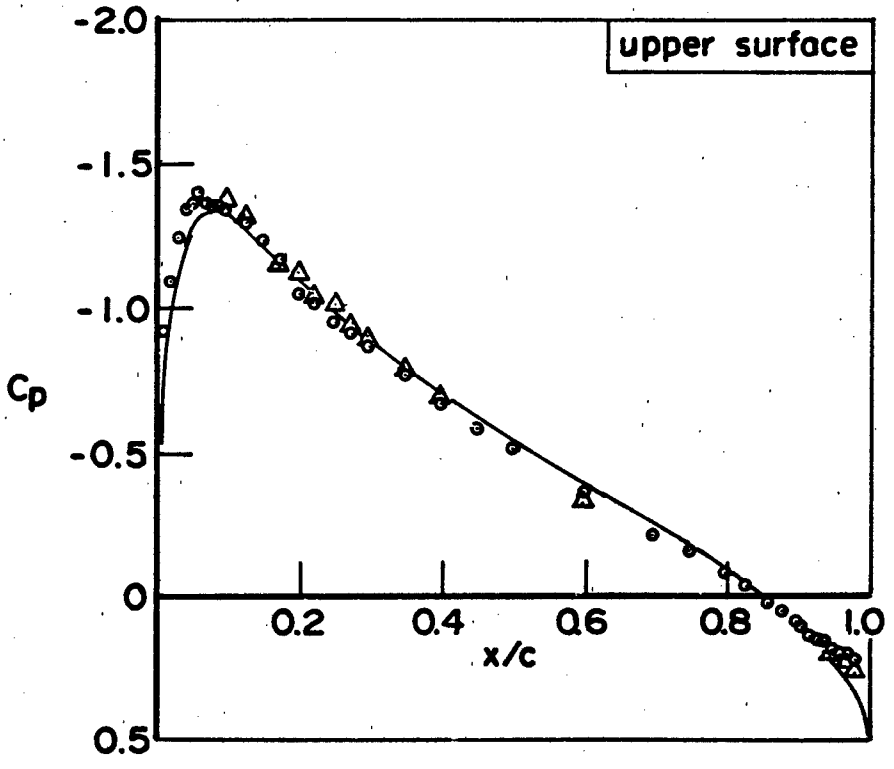

exp't.	theory (Chao)	$Re_c \times 10^{-6}$
○	—	5
△		20

$M_\infty = 0.3, \alpha = 4.5°$

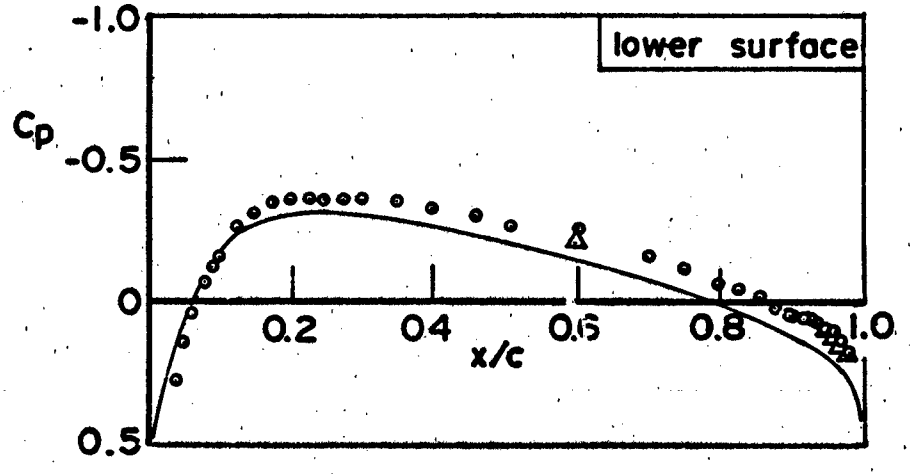

FIG. 7(b)

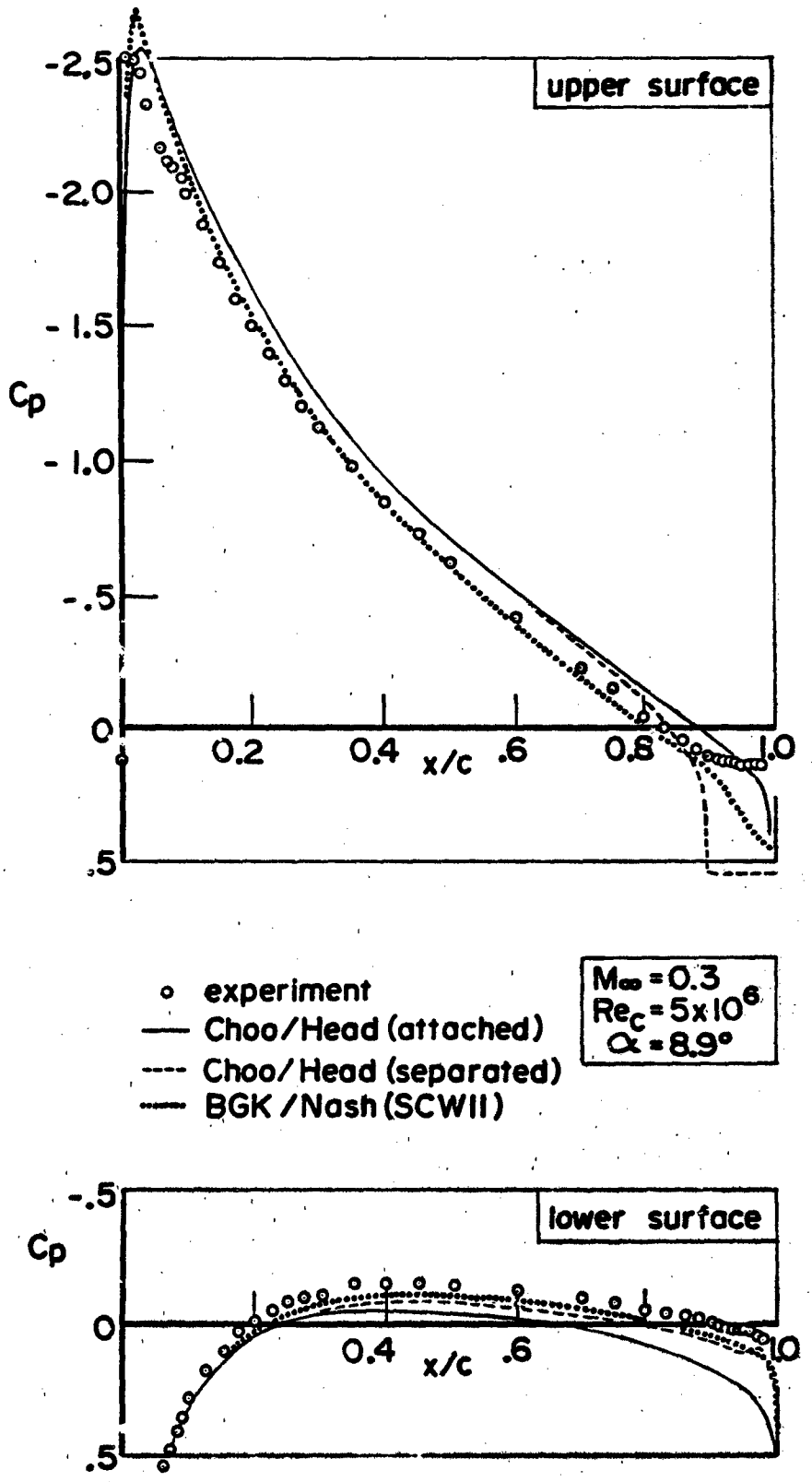
upper surface
-2.5
-2.0
- 1.5
- 1.0
-.5
0
.5
Cp
0.2
0.4
x/c
.6
0.8
1.0
o experiment
— Choo/Head (attached)
---- Choo/Head (separated)
—— BGK/Nash (SCWII)
M∞ = 0.3
Rec = 5x10^6
α = 8.9°
lower surface
-.5
0
.5
Cp
0.4
x/c
.6
1.0

FIG. 7(c)

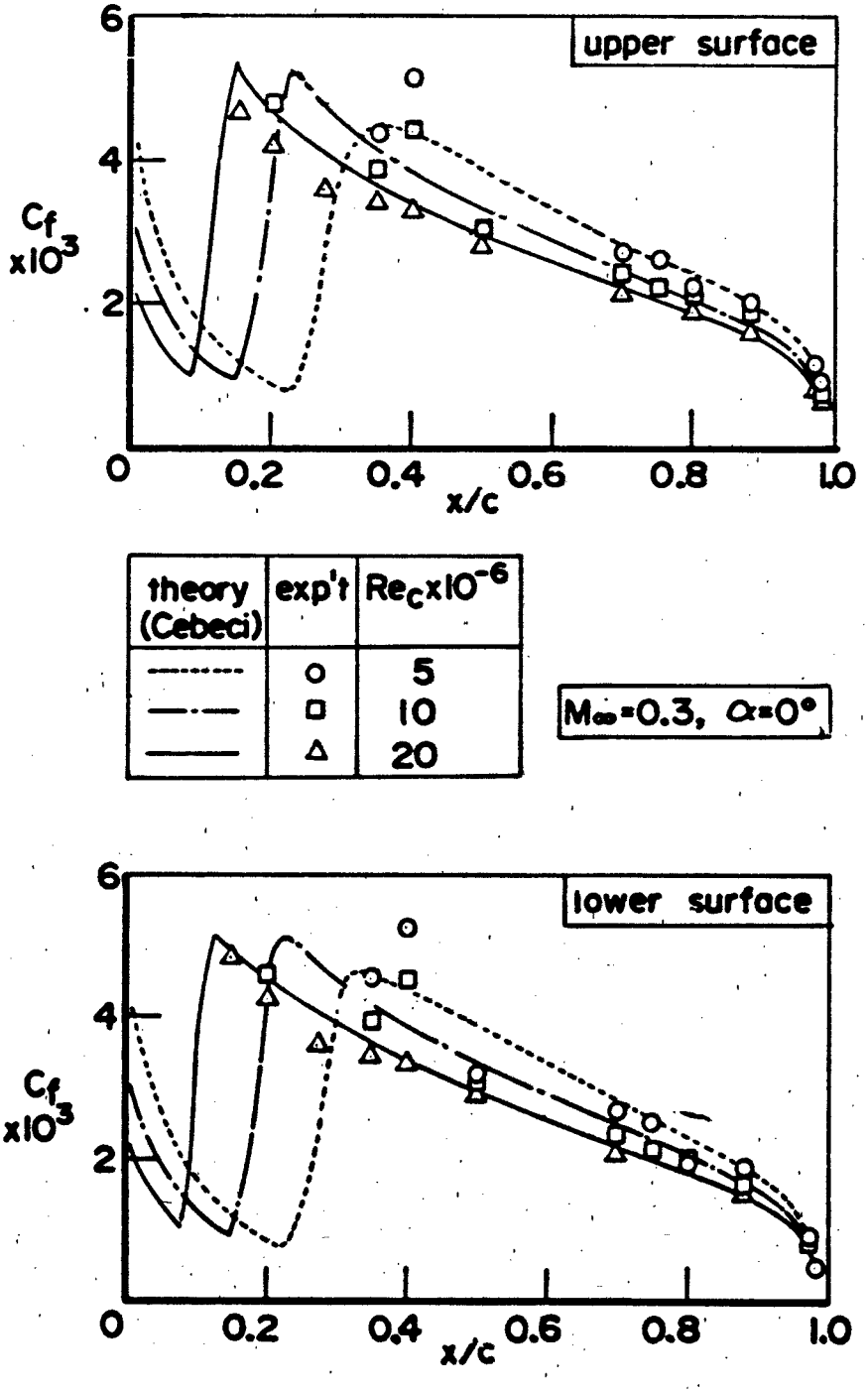

FIG. 8(a): C_f DISTRIBUTIONS — NACA 0020 MODEL, NATURAL TRANSITION

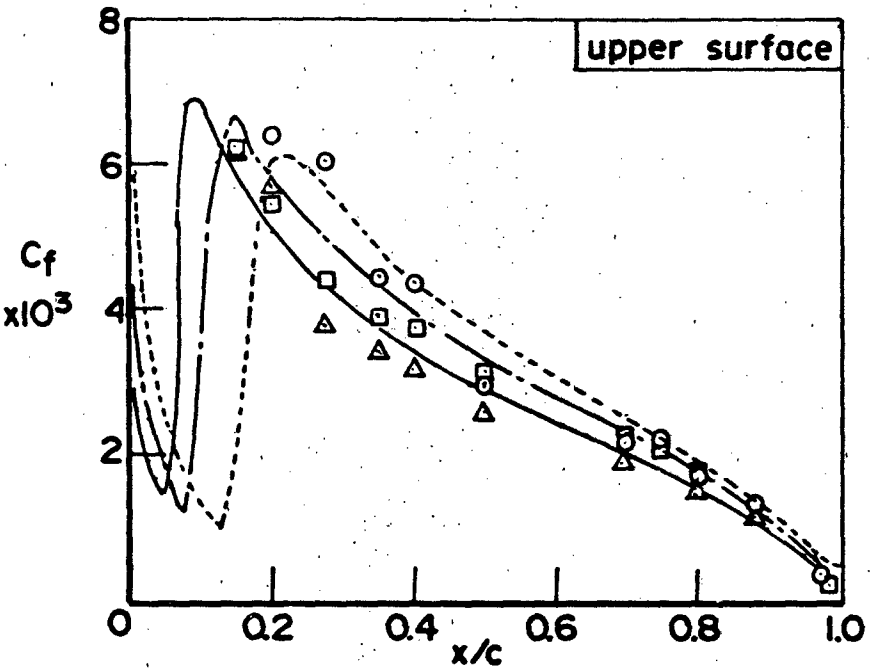

theory (Cebeci)	exp't	Re_c x 10^{-6}
-------	○	5
—·—·—	□	10
———	△	20

M_∞=0.3, α=4.5°

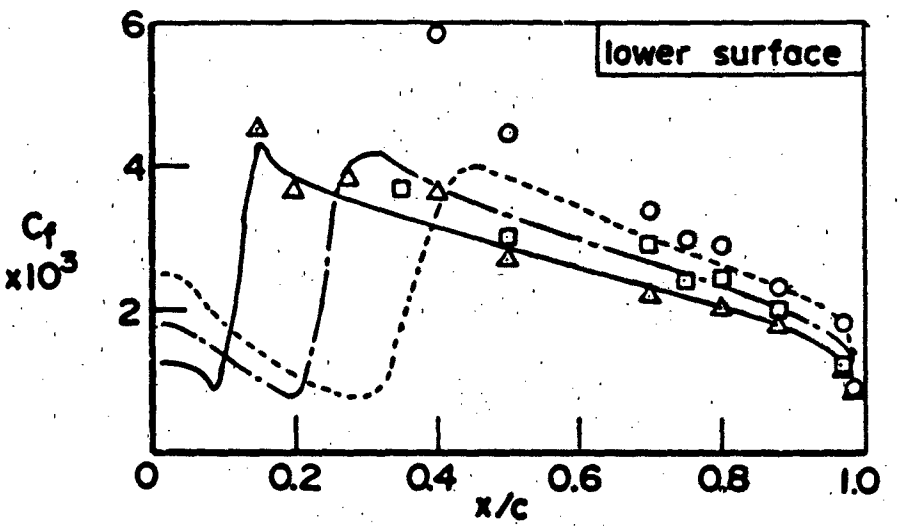

FIG. 8(b)

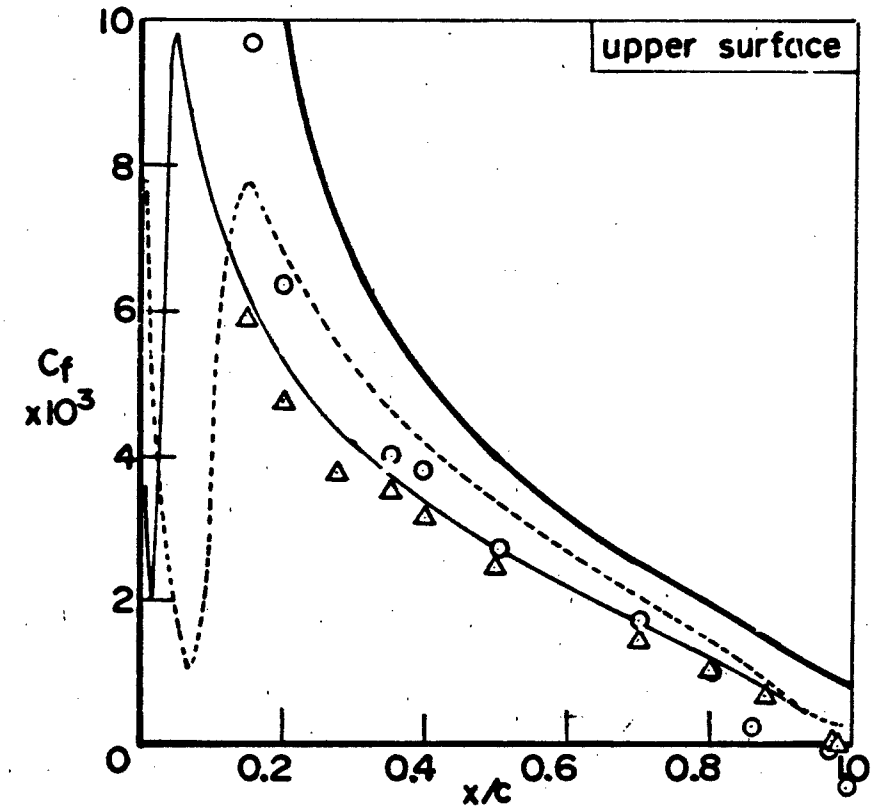

theory (Green)	theory (Cebeci)	exp't	Re_c x10^{-6}
——	------	o	5
	——	Δ	20

M_∞ = 0.3
α = 8.9°

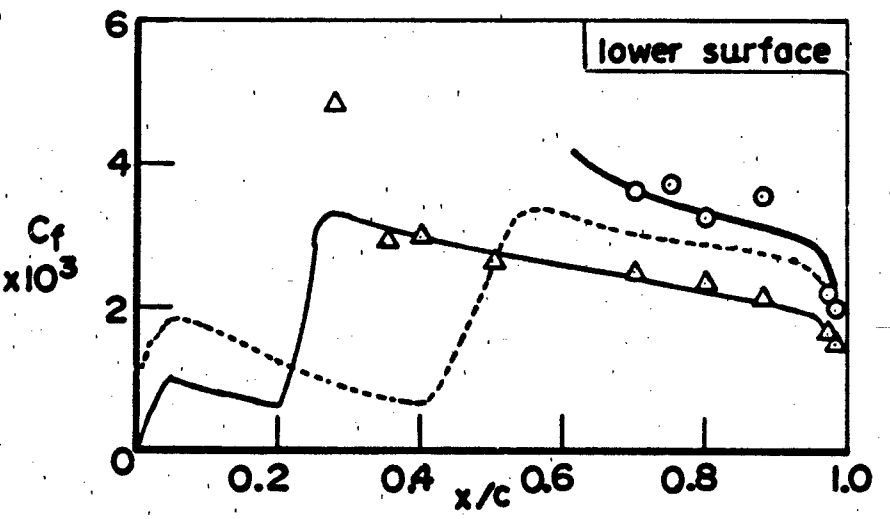

FIG. 8(c)

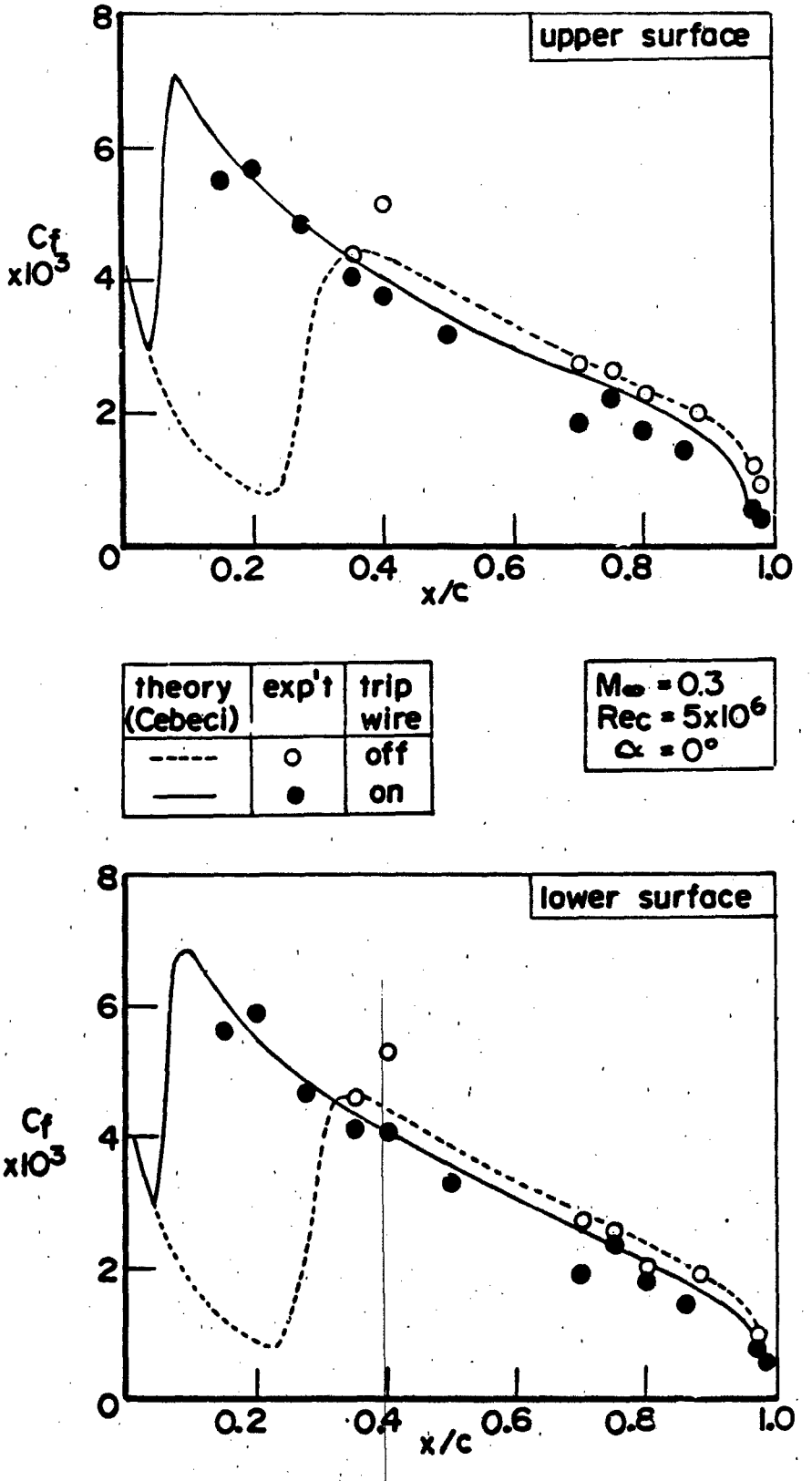

FIG. 9(a): C_f DISTRIBUTIONS — NACA 0025 MODEL, TRIPPED vs NATURAL FLOW

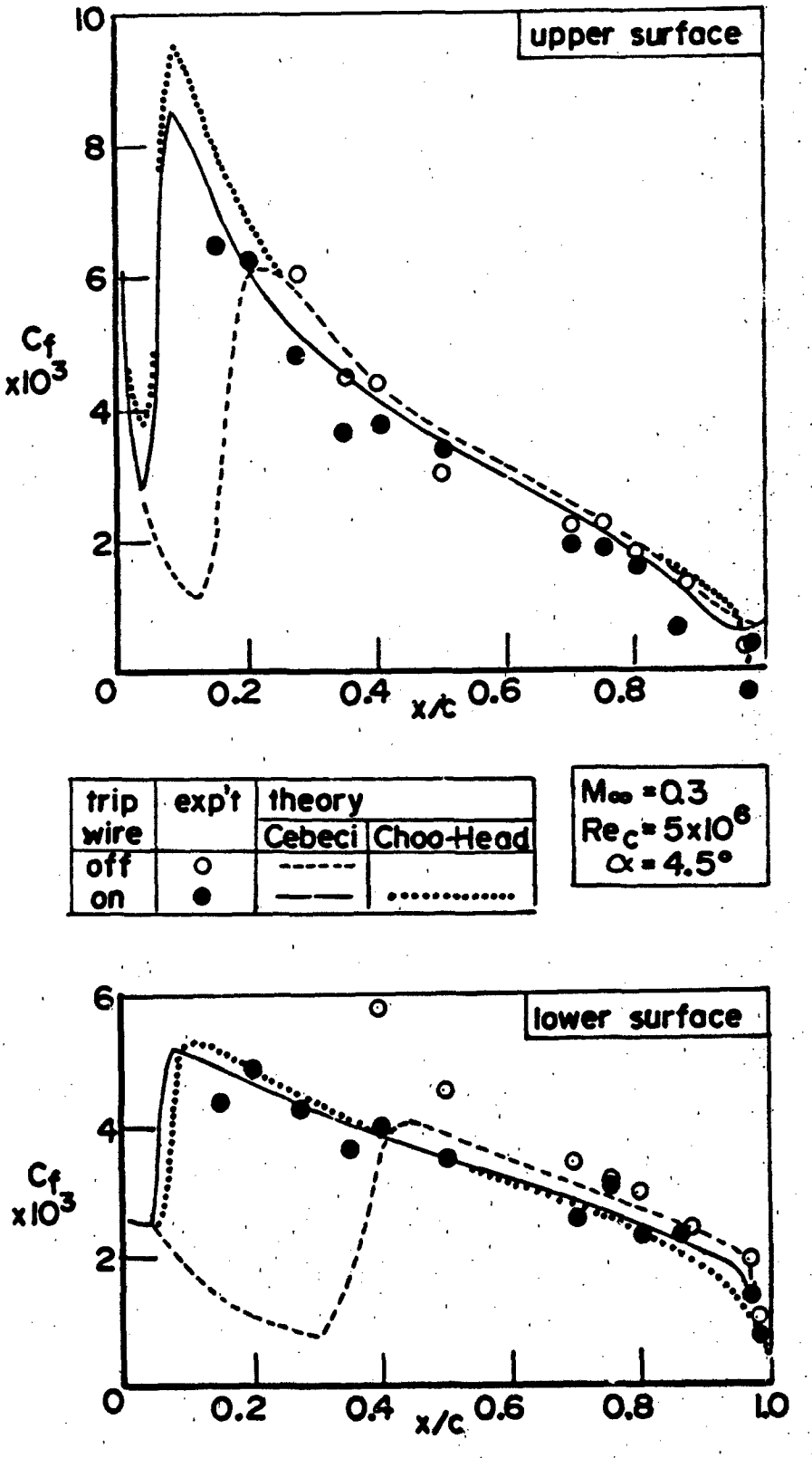
upper surface
C_f x10^3
10
8
6
4
2
0
0.2
0.4
x/c
0.6
0.8
trip wire
exp't
theory
Cebeci
Choo-Head
off
on
M_∞ = 0.3
Re_c = 5x10^6
α = 4.5°
lower surface
C_f x10^3
6
4
2
0
0.2
0.4
x/c
0.6
0.8
1.0

FIG. 9(b)

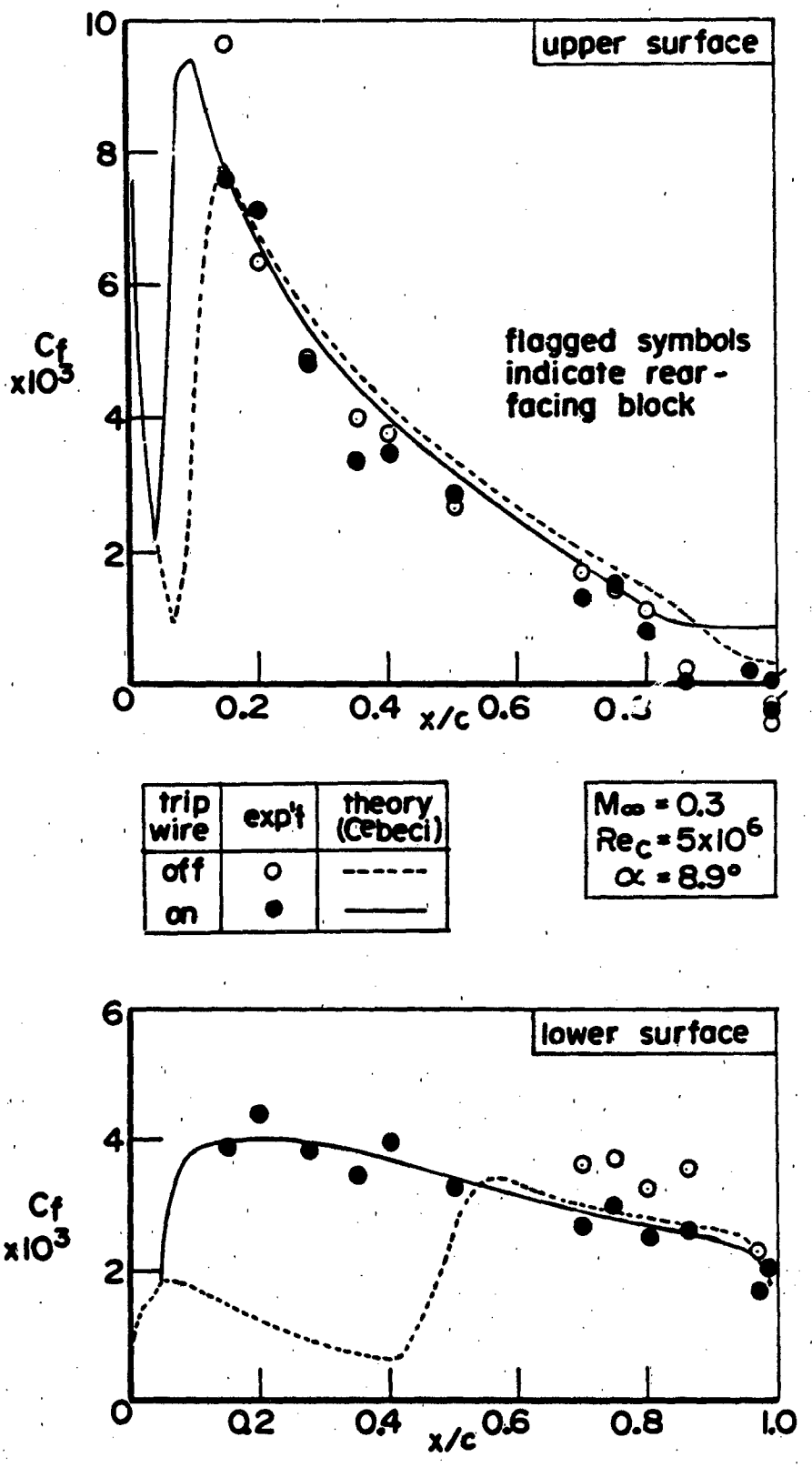
upper surface
flagged symbols indicate rear-facing block
C_f x10^3
x/c
trip wire
exp't
theory (Cebeci)
off
on
$M_\infty = 0.3$
$Re_c = 5 \times 10^6$
$\alpha = 8.9°$
lower surface
C_f x10^3
x/c

FIG. 9(c)

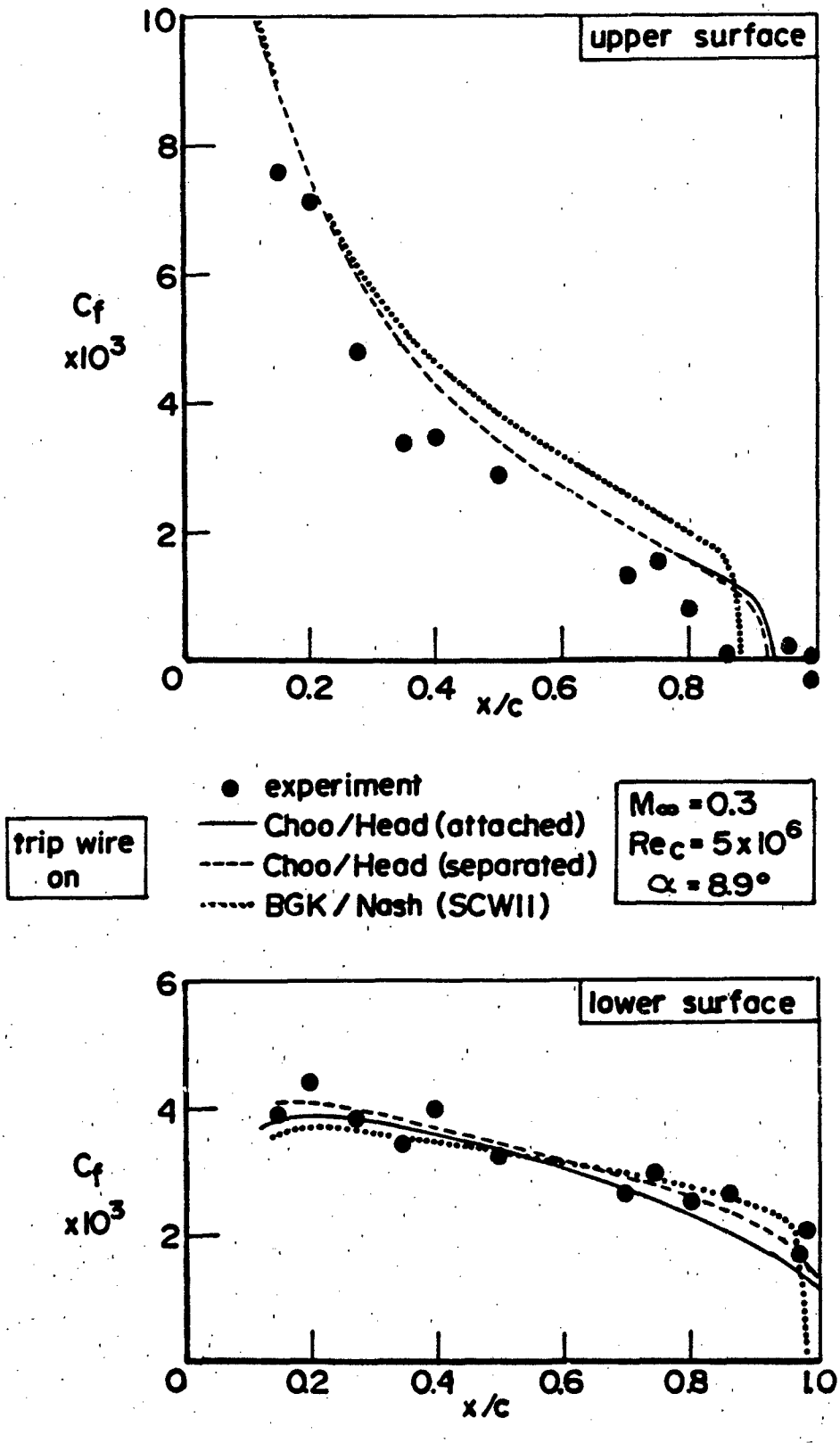
upper surface
C_f x10^3
10
8
6
4
2
0
0.2
0.4
x/c
0.6
0.8
trip wire on
experiment
Choo/Head (attached)
Choo/Head (separated)
BGK / Nash (SCW11)
M_∞ = 0.3
Re_c = 5x10^6
α = 8.9°
lower surface
C_f x10^3
6
4
2
0
0.2
0.4
x/c
0.6
0.8
1.0

FIG. 9(d)

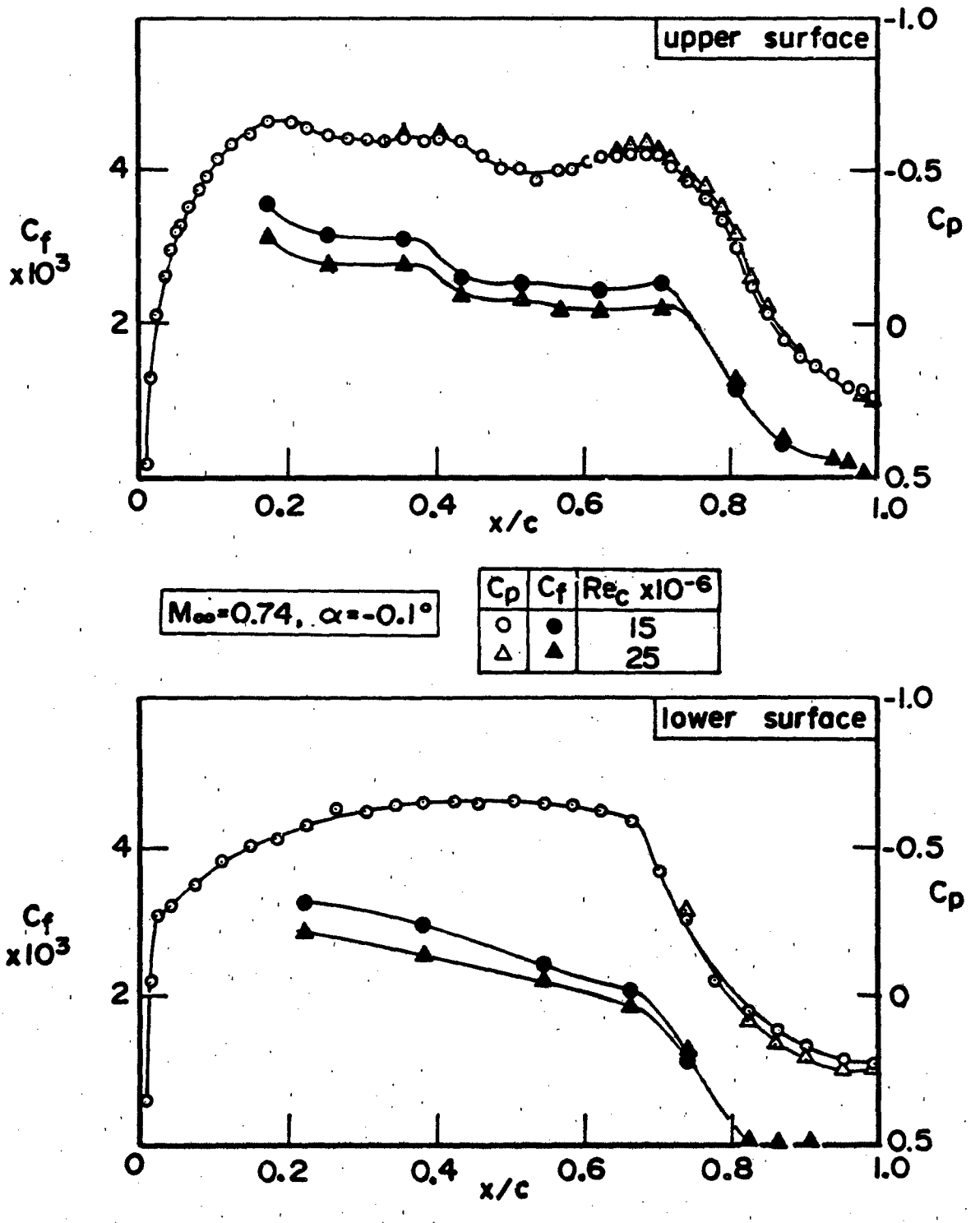

FIG. 10(a): C_f DISTRIBUTIONS — SUPERCRITICAL AIRFOIL MODEL

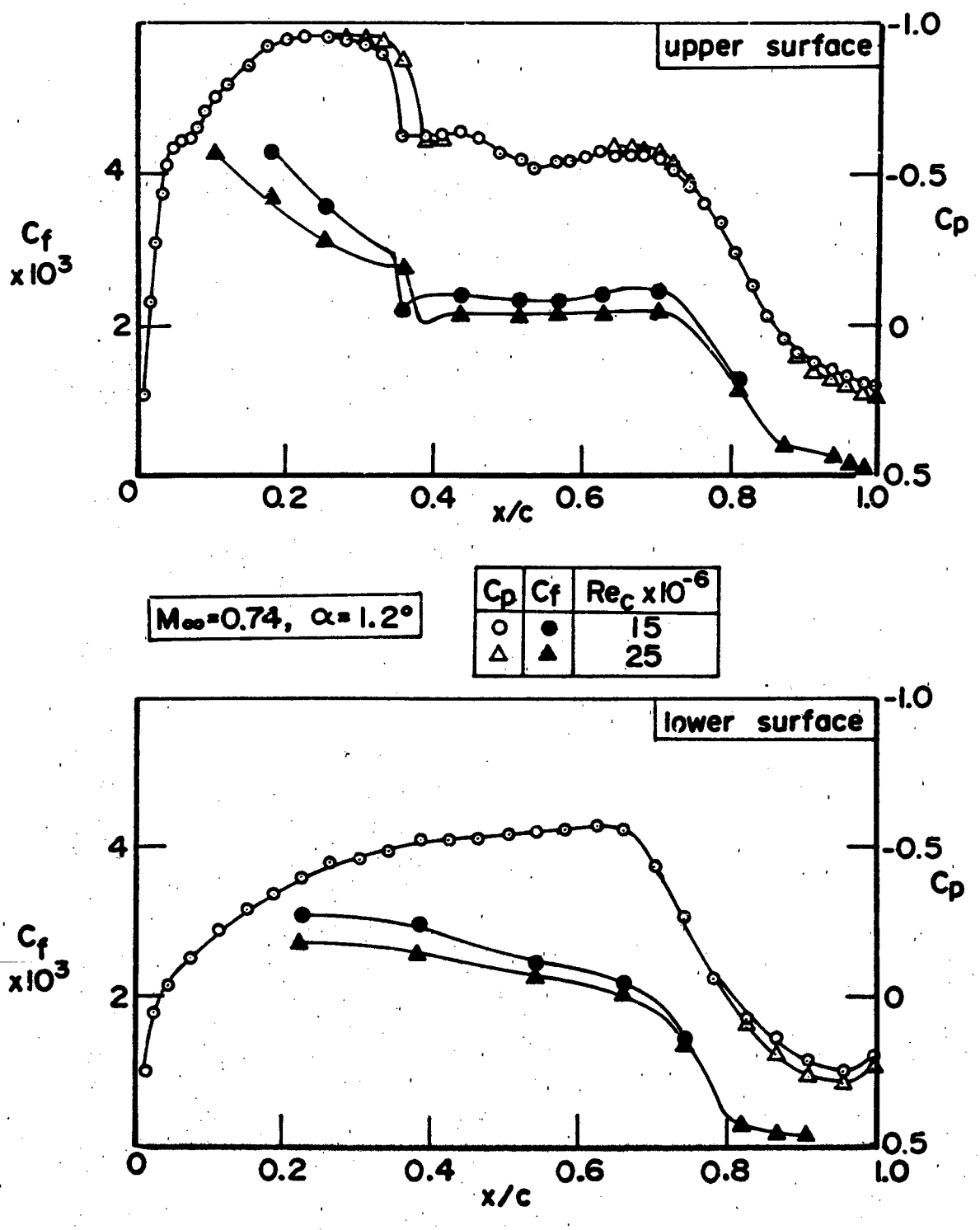
upper surface
lower surface
C_f x10^3
C_p
x/c
0
0.2
0.4
0.6
0.8
1.0
2
4
-1.0
-0.5
0
0.5
M_∞=0.74, α= 1.2°
C_p C_f Re_c x10^{-6}
○ ● 15
△ ▲ 25

FIG. 10(b)

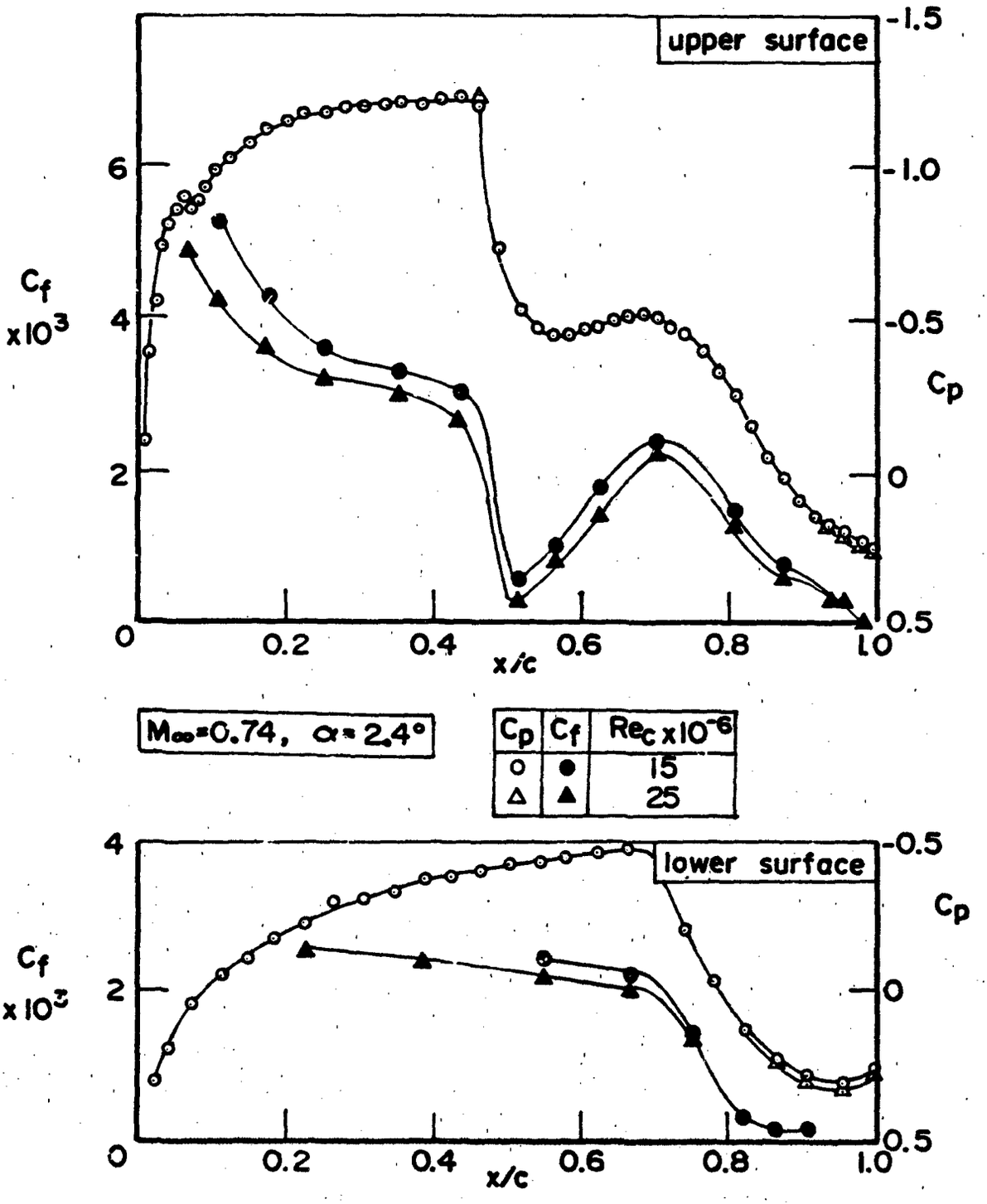
upper surface
lower surface
C_f x10^3
C_p
x/c
M_∞=0.74, α= 2.4°
C_p | C_f | Re_c x10^{-6}
0 | ● | 15
△ | ▲ | 25

FIG. 10(c)

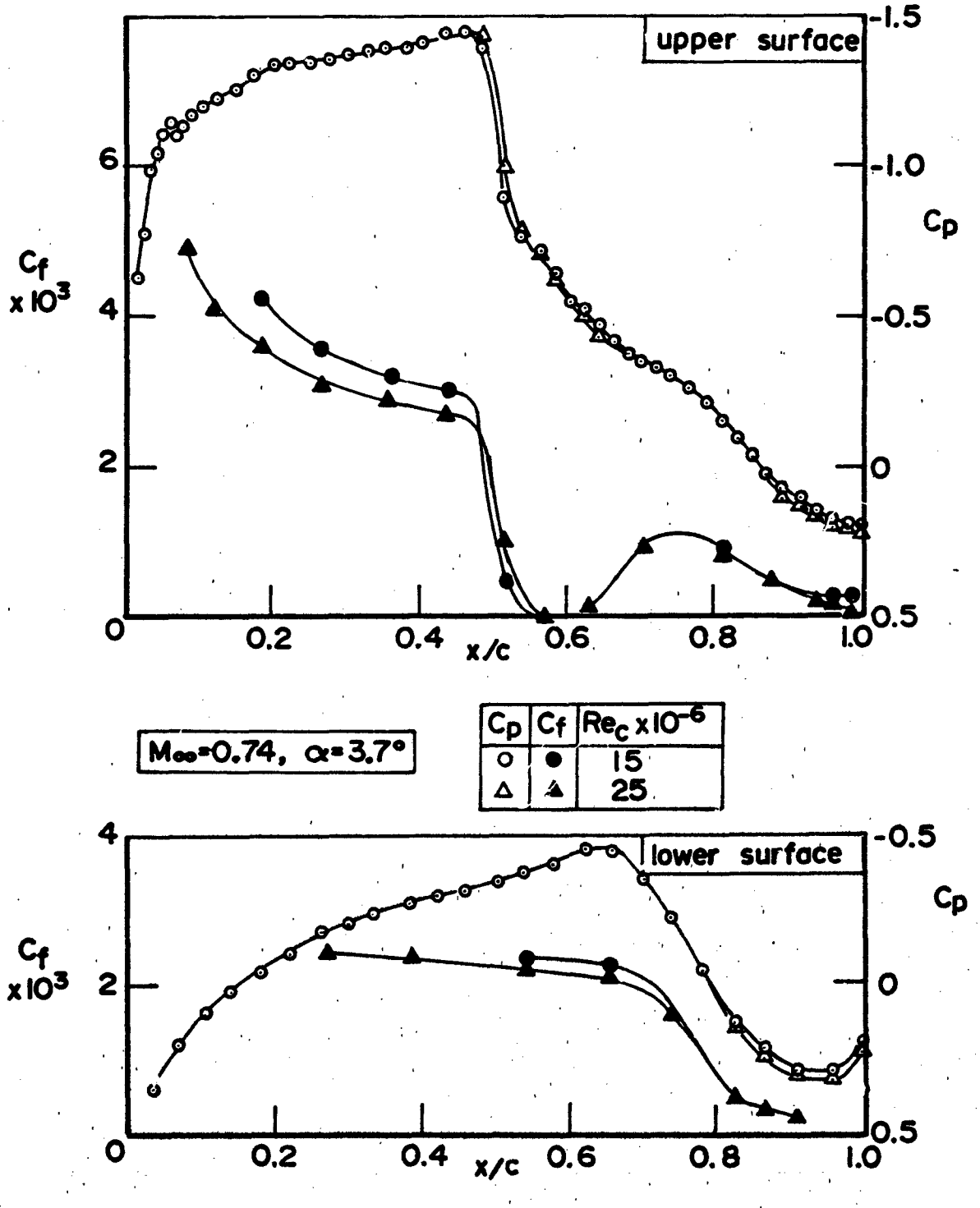
upper surface
lower surface
$C_f \times 10^3$
C_p
x/c
M_∞=0.74, α=3.7°
C_p C_f $Re_c \times 10^{-6}$
15
25

FIG. 10(d)

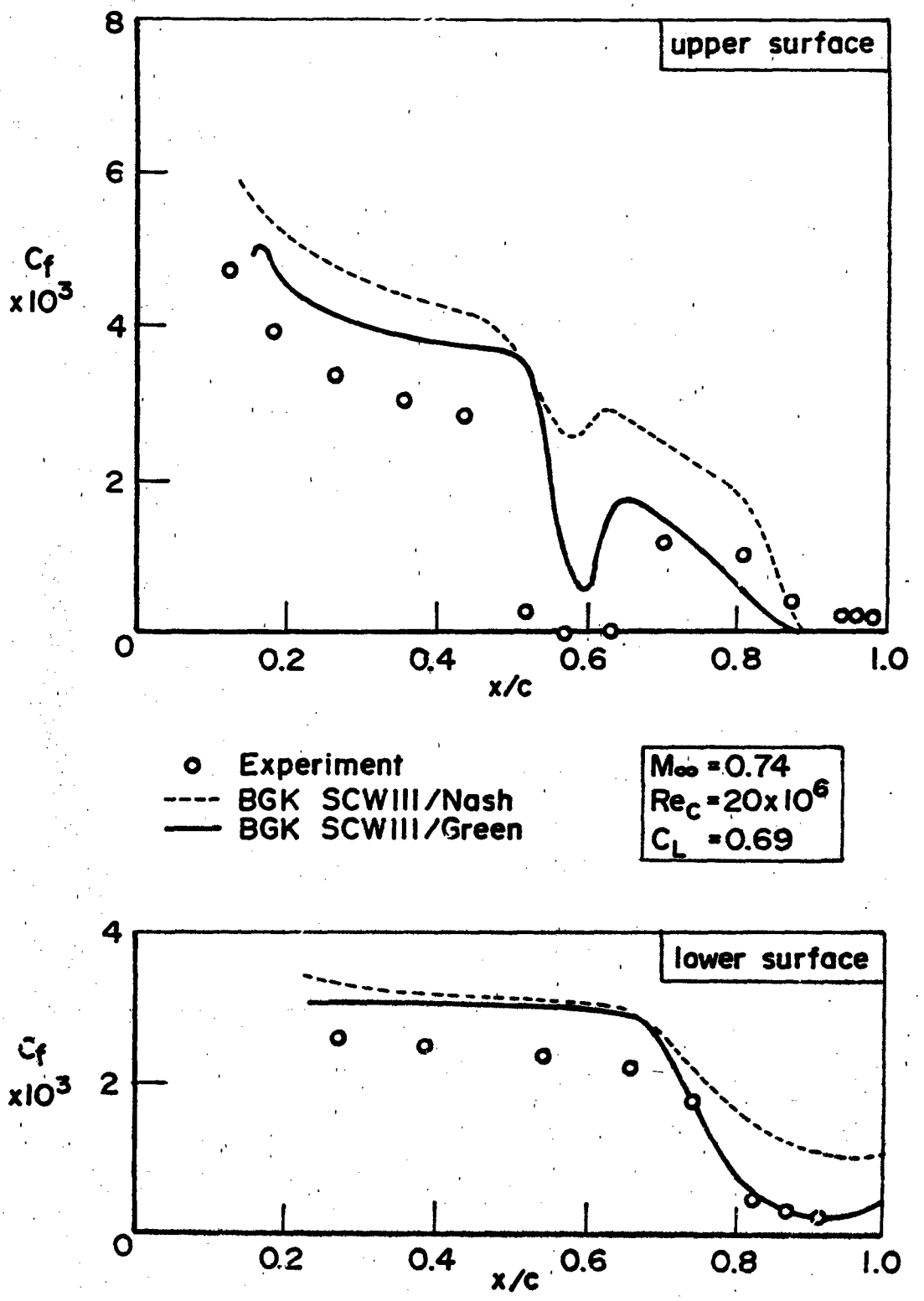

FIG. 11: C_f DISTRIBUTION AT HIGH LIFT

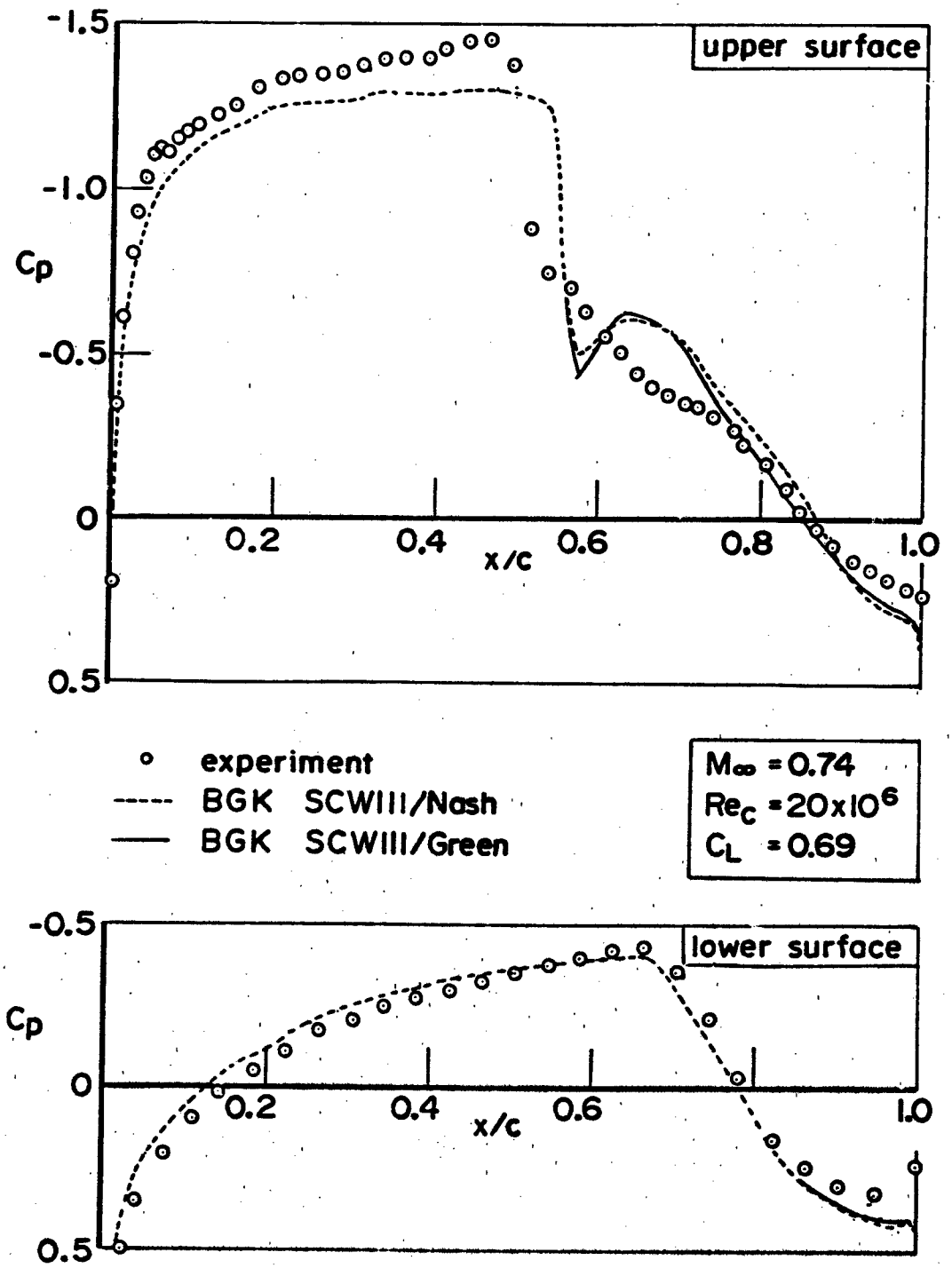

FIG. 12: C_p DISTRIBUTIONS AT HIGH LIFT

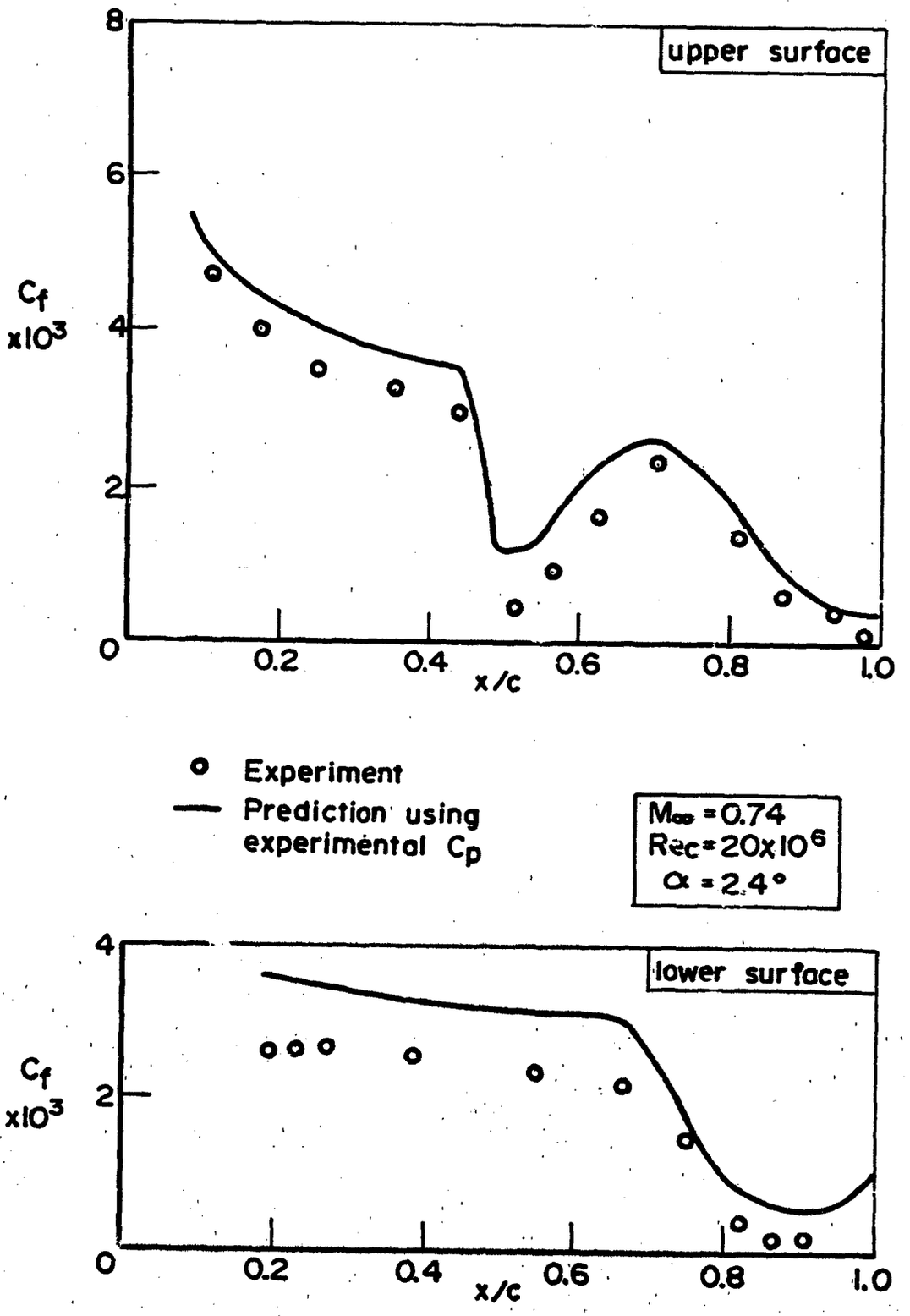

FIG. 13: CHECK ON GREEN'S C_f PREDICTION

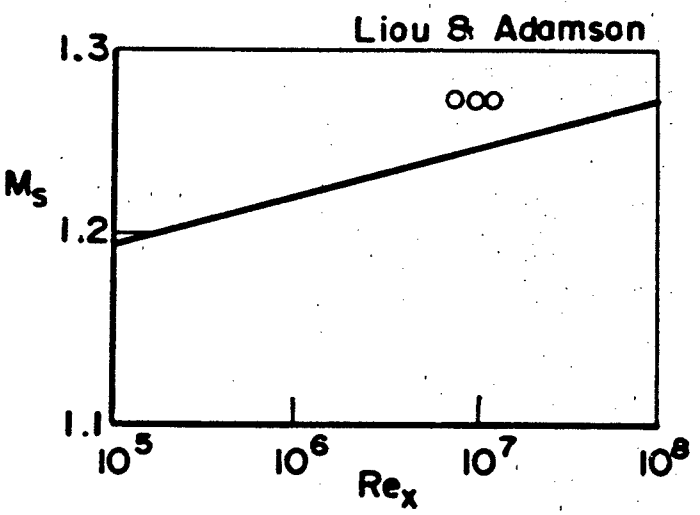

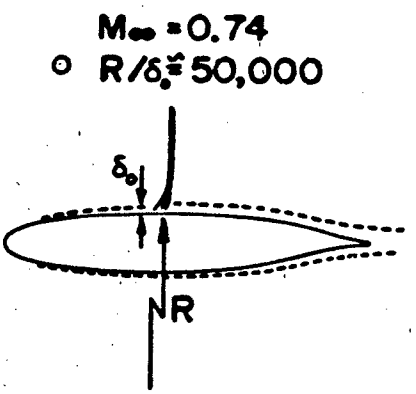

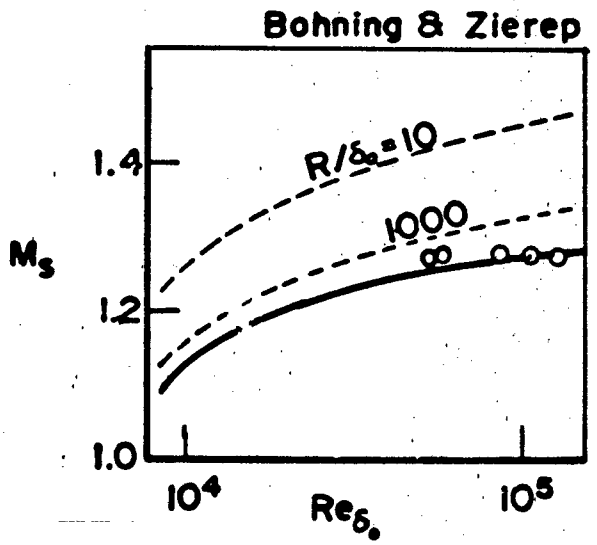

FIG. 14: INCIPIENT SEPARATION UNDER A NORMAL SHOCK WAVE

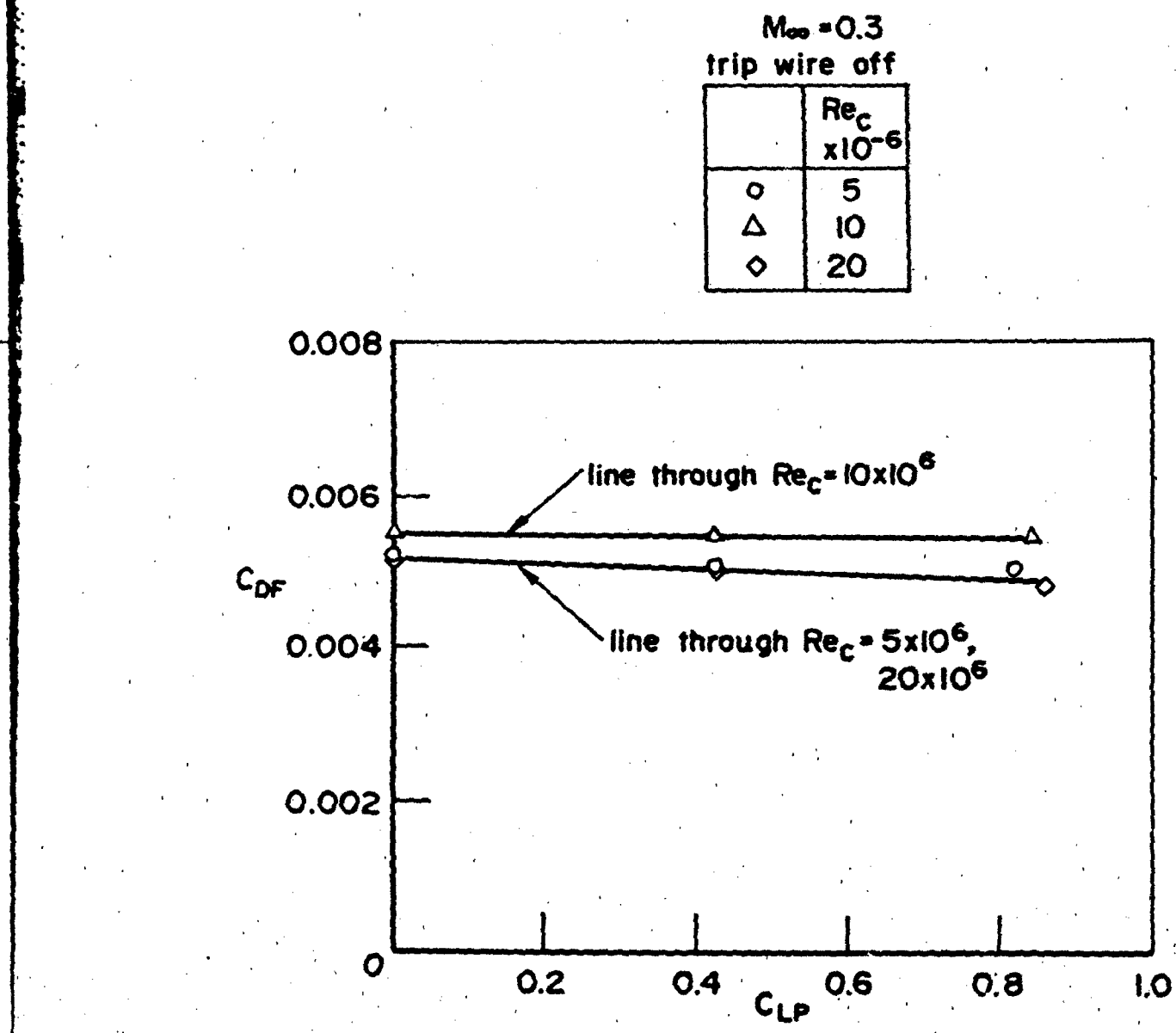

FIG. 15(a): SKIN FRICTION DRAG – NACA 0020 AIRFOIL

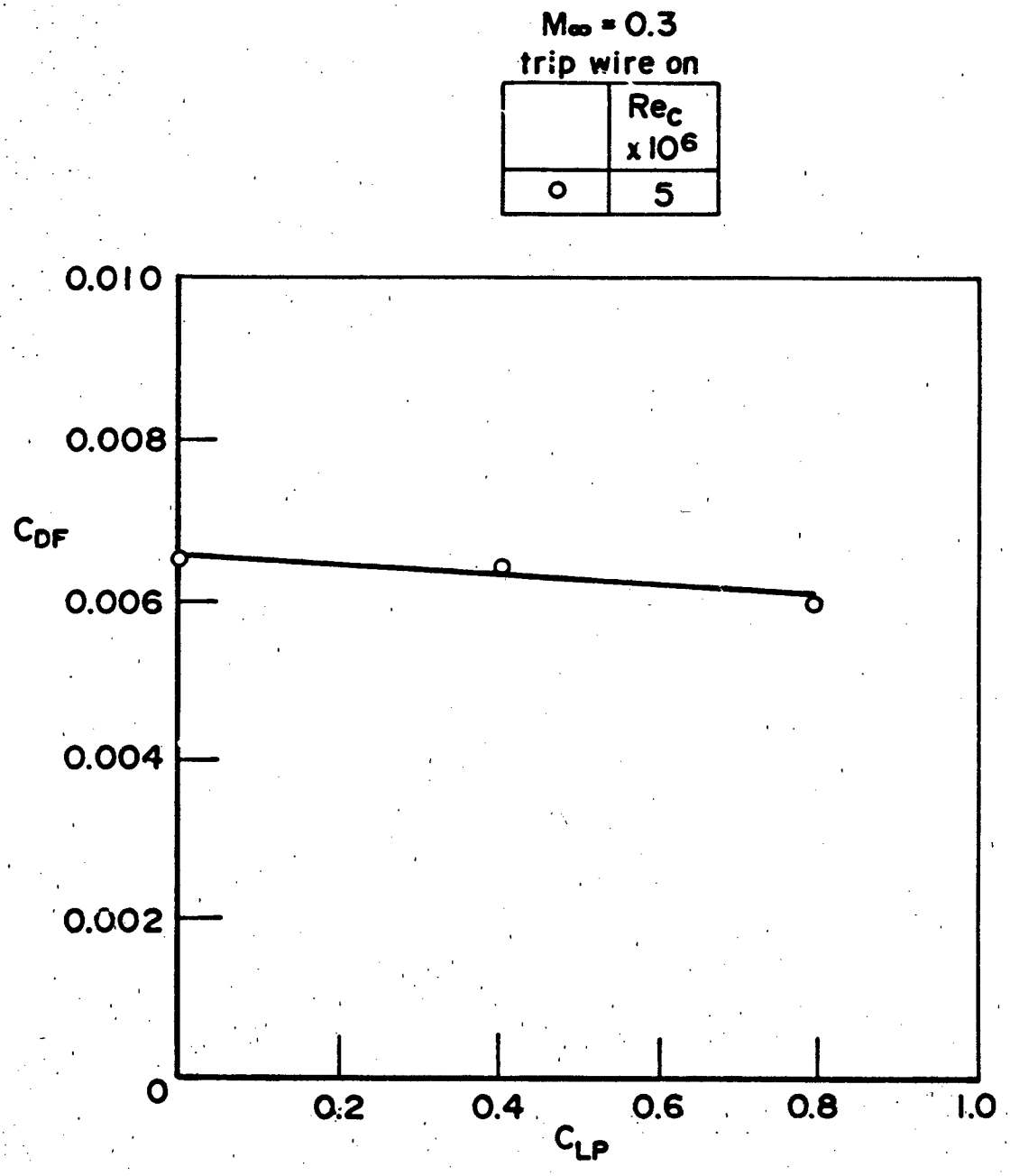
M∞ = 0.3
trip wire on
Re_C x 10^6
5
0.010
0.008
0.006
0.004
0.002
0
C_DF
0.2
0.4
0.6
0.8
1.0
C_LP

FIG. 15(b)

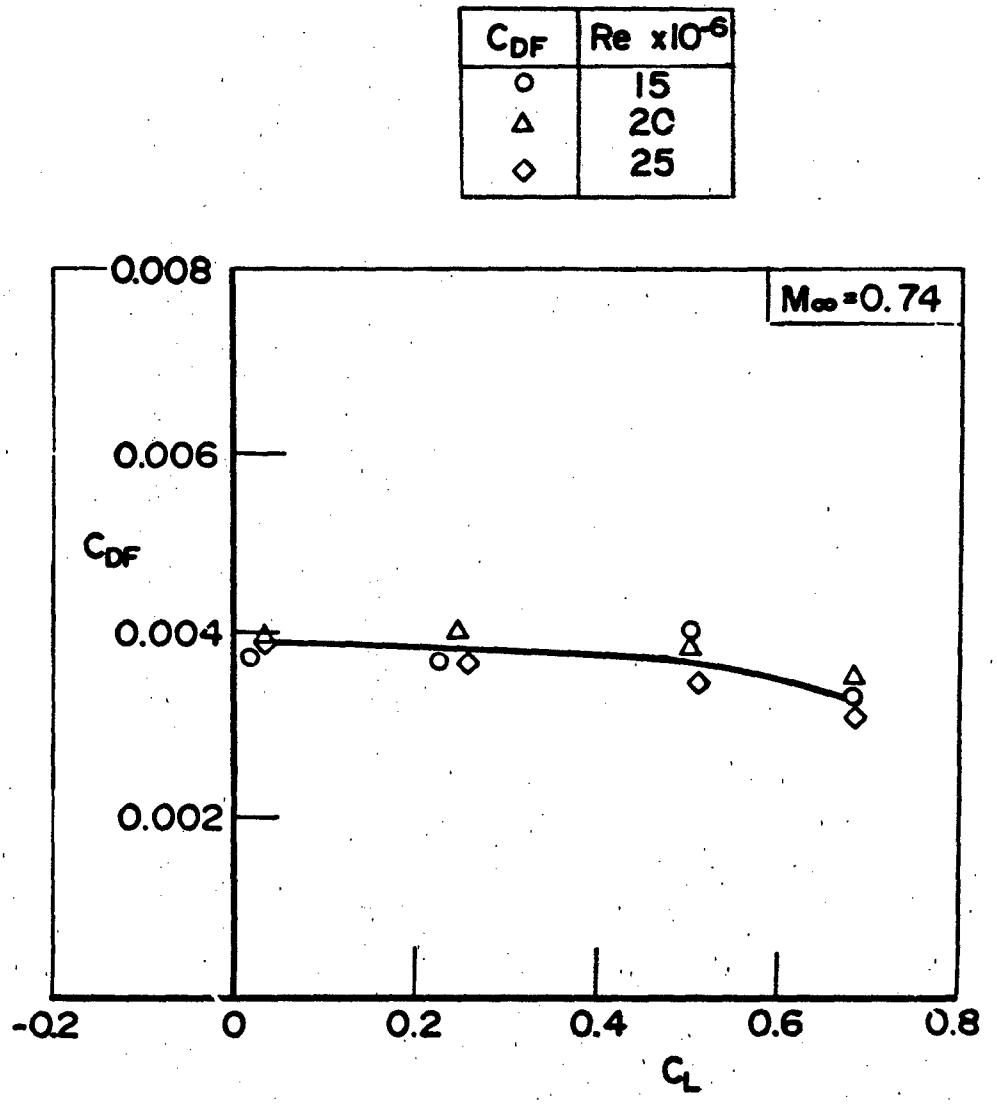

FIG. 16: SKIN FRICTION DRAG — SUPERCRITICAL AIRFOIL

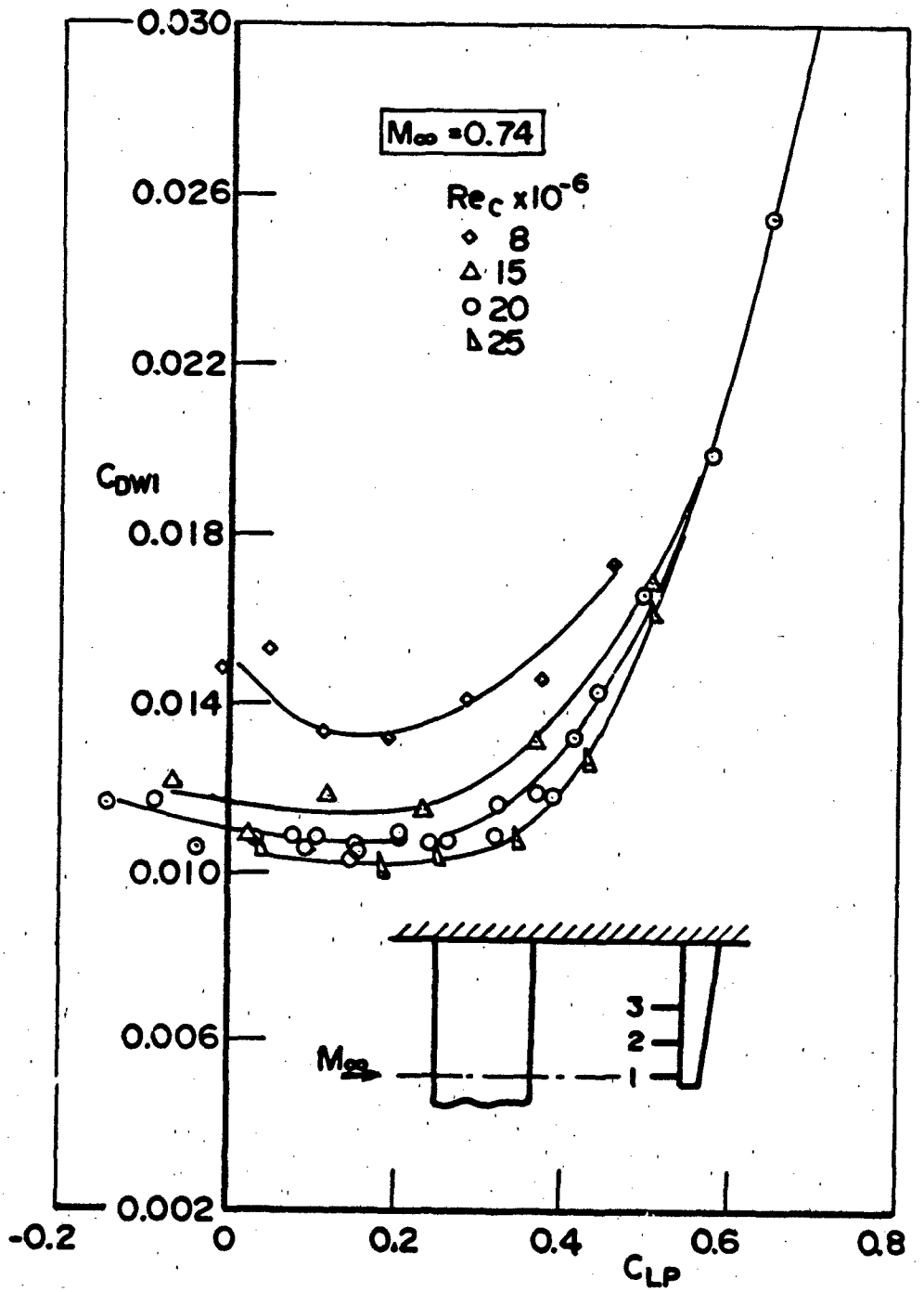

FIG. 17: DRAG INDICATED BY CENTRELINE PITOT — SUPERCRITICAL AIRFOIL

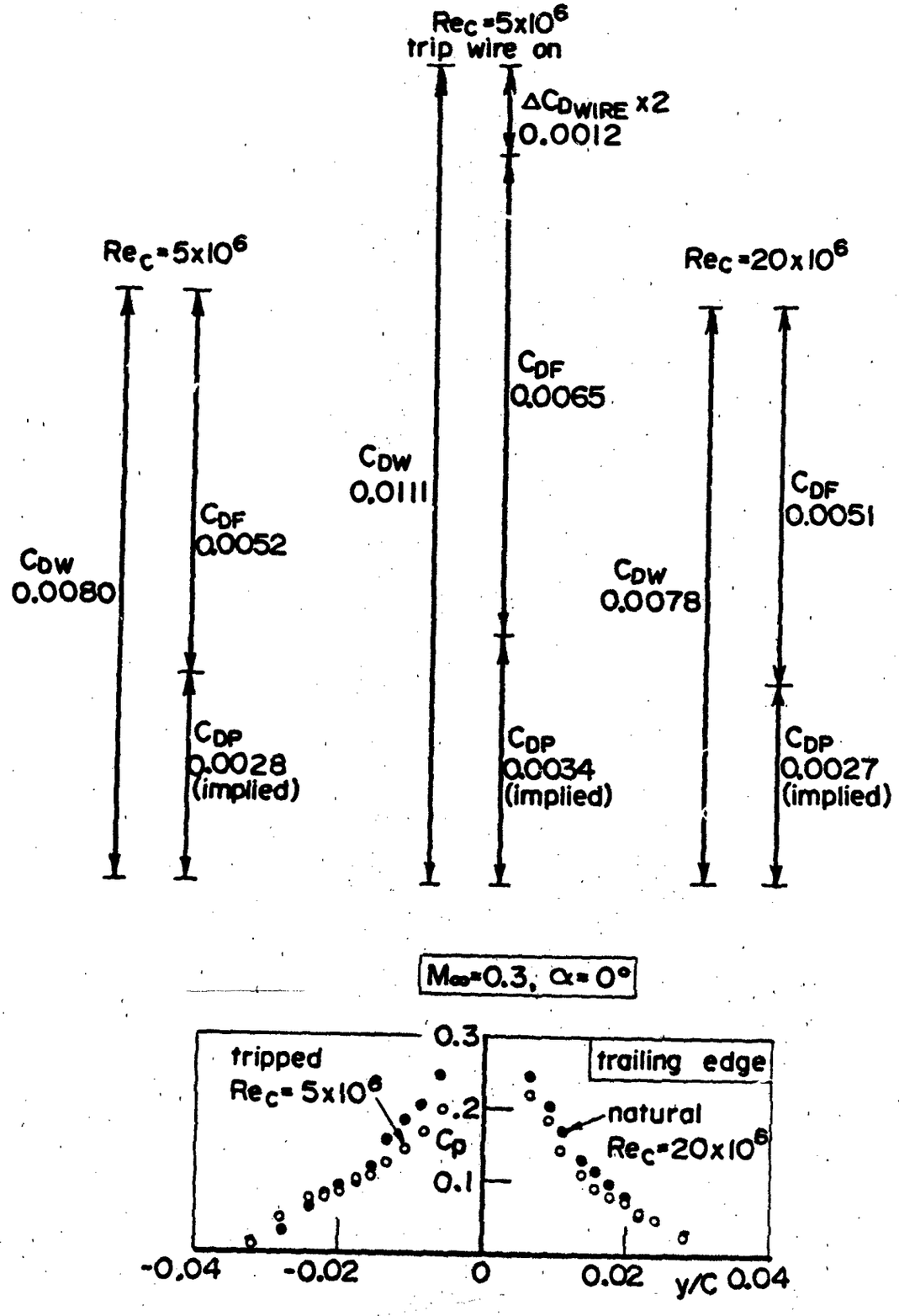

FIG. 18: COMPONENTS OF TOTAL DRAG -- NACA 0020 AIRFOIL

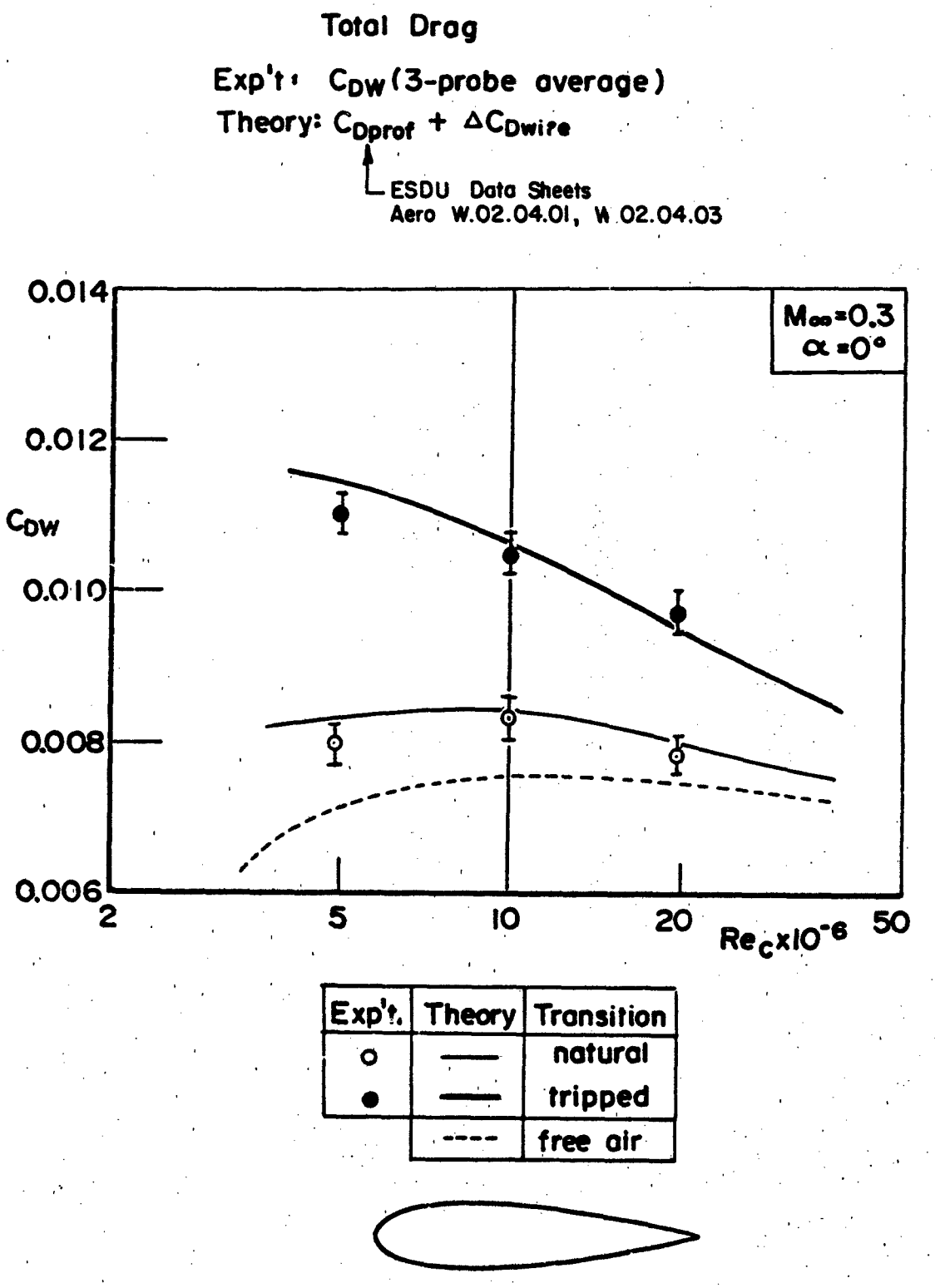

FIG. 19: DRAG PREDICTIONS — NACA 0020 AIRFOIL

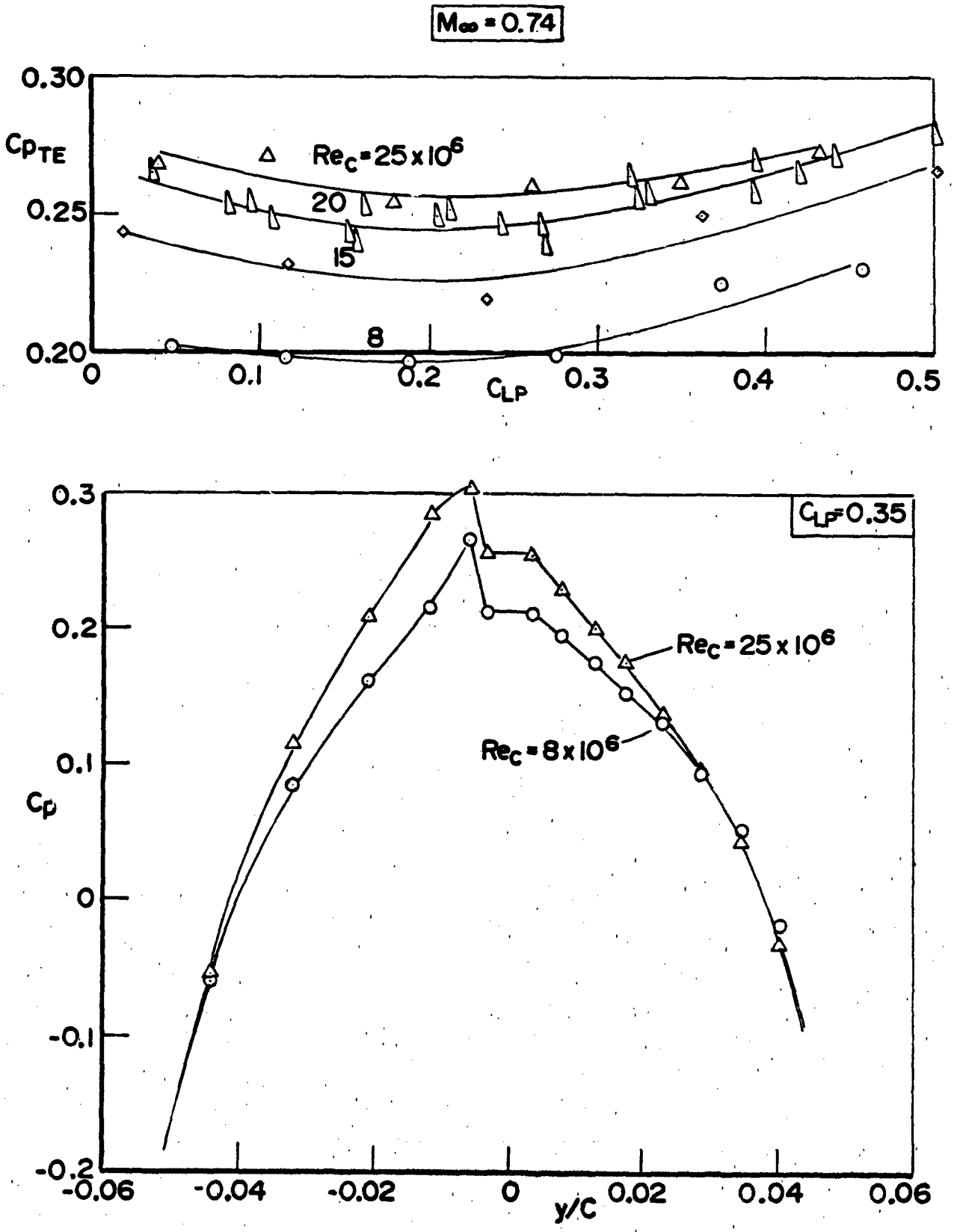

FIG. 20: ORIGIN OF C_{DP} VARIATION WTH Re_c

APPENDIX I

DETERMINATION OF BOUNDARY LAYER TRANSITION USING THE CORRELATION OF VAN DRIEST & BLUMER

The following steps were taken for a given airfoil:

1. The leading edge stagnation point was determined by interpolation of the measured surface pressure distribution.

2. For each pressure orifice location, the arc length, s, and Reynolds number Re_s, based on distance from the stagnation point were calculated. This was done for both upper and lower surfaces.

3. Starting from the stagnation point, the local Falkner-Skan exponent, m was determined at each orifice location. This calculation was performed by using a three-point Lagrange interpolation (see, for example, Cebeci & Bradshaw, p. 260) on the local velocity at the boundary layer edge U_e, derived from the local Cp measurement. At this point we have then a local fit, $U_e \cong cS^m$, where 'c' and 'm' are constants.

4. The equivalent Falkner-Skan non-dimensional laminar boundary layer thickness, tabulated by Van Driest, was curve-fitted as: $\eta = 5.18 - 8.02\,m + 8.2\,m^2$.

5. The transition Reynolds number, Re_{TR}, at each static orifice location is found by solving the relation given by Van Driest

$$\frac{1690}{\sqrt{Re_{TR}}} = 0.312\,(m + 0.11)^{-0.528} + 0.73\,(\eta \cdot u'/U_\infty)^2 \sqrt{Re_{TR}}$$

where u'/U_∞ is the freestream turbulence level.

6. Marching downstream from the stagnation point, the start of transition was taken to be at the first orifice location where $Re_{TR} < Re_s$.

REPORT DOCUMENTATION PAGE / PAGE DE DOCUMENTATION DE RAPPORT

REPORT/RAPPORT 1a	REPORT/RAPPORT 1b
NAE-AN-23	NRC No. 23941
REPORT SECURITY CLASSIFICATION / CLASSIFICATION DE SÉCURITÉ DE RAPPORT 2	**DISTRIBUTION (LIMITATIONS) 3**
Unclassified	Unlimited

TITLE/SUBTITLE/TITRE/SOUS-TITRE 4

Skin Friction Measurements ~~on~~ FOR Two Relatively Thick Airfoil Sections at High Reynolds Number

AUTHOR(S)/AUTEUR(S) 5

G.M. Elfstrom

SERIES/SÉRIE 6

Aeronautical Note

CORPORATE AUTHOR/PERFORMING AGENCY/AUTEUR D'ENTREPRISE/AGENCE D'EXÉCUTION 7

National Research Council Canada
National Aeronautical Establishment — High Speed Aerodynamics Laboratory

SPONSORING AGENCY/AGENCE DE SUBVENTION 8

DATE 9	FILE/DOSSIER 10	LAB. ORDER / COMMANDE DU LAB. 11	PAGES 12a	FIGS/DIAGRAMMES 12b
84-11			77	20

NOTES 13

DESCRIPTORS (KEY WORDS)/MOTS-CLÉS 14

1. Skin friction drag

SUMMARY/SOMMAIRE 15

An experimental investigation of turbulent skin friction for two airfoil sections under conditions of high Reynolds number is described. Data are presented for an NACA 0020 section at a Mach number of 0.30 and chord Reynolds numbers between 5 and 20 million, and for a 16% thick supercritical section at a Mach number of 0.74 and chord Reynolds numbers between 15 and 25 million. Together with estimates of boundary layer transition location, these data are integrated to determine the skin friction component of total drag. The results are then discussed in terms of observed variation of total drag with Reynolds number.